A Data-Driven Analysis to Determine the Electrical Needs of a Hybrid Powertrain System for Small, Hyper-Optimized, Track-Day Vehicles

by

Henry J. Asa

Submitted to the Department of Mechanical Engineering
in partial fulfillment of the requirements for the degree of

BACHELOR OF SCIENCE IN MECHANICAL ENGINEERING

at the

MASSACHUSETTS INSTITUTE OF TECHNOLOGY

May 2024

Authored by:	Henry J. Asa Department of Mechanical Engineering May 30, 2024
Certified by:	Amos G. Winter Professor of Mechanical Engineering, Thesis Supervisor
Accepted by:	Kenneth Kamrin Professor of Mechanical Engineering Undergraduate Officer, Department of Mechanical Engineering

A Data-Driven Analysis to Determine the Electrical Needs of a Hybrid Powertrain System for Small, Hyper-Optimized, Track-Day Vehicles

by

Henry J. Asa

Submitted to the Department of Mechanical Engineering
on May 30, 2024 in partial fulfillment of the requirements for the degree of

BACHELOR OF SCIENCE IN MECHANICAL ENGINEERING

ABSTRACT

In an effort to maximize the performance of RUSH Auto Work's RUSH SR racecar, a hybrid powertrain system was designed and evaluated to estimate the performance gains from implementing such a system. An extensive Python program was developed to analyze real-world race data for the RUSH SR, determining energy losses while braking, the vehicle's current acceleration capabilities, as well as the vehicle's limitations. This ultimately quantified the vehicle's current performance values/capabilities, and provided a strong foundation for the analyses that determined the anticipated implications of adding a hybrid powertrain system to the car. Despite the mass additions associated with adding an electric motor, battery pack, and additional components to control the system, the power gains from the system yielded a net greater power-to-weight ratio than the original vehicle without the hybrid system. An analysis of energy recuperation through regenerative braking demonstrated the potential to reduce the size of the battery pack (which decreases the mass of the system) without compromising on the power requirements and capabilities of the system. During periods of heavy braking, it was found that a significant portion of the battery could be recharged, allowing for significant reductions in the capacity of the battery pack.

Thesis supervisor: Amos G. Winter

Title: Professor of Mechanical Engineering

Acknowledgments

Thank you to Professor Amos Winter for his supervision and guidance on this thesis project. The opportunity to work with RUSH Auto Works was an incredible opportunity, and I am grateful to have been able to work with Mr. David Hosie, Mr. Blair Hosie, and Mr. Patrick McGabe on this project. Additionally, Ms. Ashley English and Mr. Anthony Altala were invaluable partners in navigating this research project.

Contents

List of Figures

List of Tables

Chapter 1

Introduction

This section introduces RUSH Auto Works Inc. in section 1.1 and the RUSH SR motorsports vehicle in section 1.2, providing necessary context for the philosophy of the research and the nature of the vehicle being used. Section 1.4 outlines the goals of the thesis project, as well as the main requirements that needed to be addressed.

1.1   Overview of RUSH Auto Works Inc.

RUSH Auto Works Inc. was founded in 2017 by David Hosie, a mechanical engineer with over 40 years of experience in engineering design, development, and product manufacturing. From the onset of the company, RUSH has pushed the envelope of vehicle performance and affordability. With the goal of designing, developing, and producing affordable, high-performance race and track-day motorsports vehicles, RUSH has rapidly established a prominent name for itself within the motorsports industry. The company's ethos revolves around the idea that every vehicle they build will deliver a thrilling driving experience.

Inspired by the engineering principles of Lotus Cars and its founder Colin Chapman, RUSH Auto Works strives to develop racecars that embodies simplicity and lightness. These goals are evident in their first car, the RUSH SR which packs over 140 horsepower into a 513 kilogram car.

Operating out of a facility in Houston, Texas, RUSH produces many of the parts for the SR in-house, helping the company drive costs down and deliver exceptional performance to its customers [1].

1.2   RUSH SR Vehicle

The RUSH SR is the company's flagship product, delivering over 140 horsepower and a top speed of around 152 miles per hour for the price of $39,875.

The vehicle's design process focused on minimizing costs without compromising performance. For example, instead of using expensive off-the-shelf dampers, engineers at RUSH developed in-house alternatives. This approach extends to many other components in the car, like the steering rack and limited-slip differential, ensuring affordability and performance.

Despite prioritizing keeping the vehicle lightweight, RUSH did not compromise on fragility, a frequently associated drawback of high-performance racing cars. A fiberglass body provides rigidity and strength for the car without sacrificing strength and durability.

Figure 1.1: RUSH SR Sportscar [2].

The chassis uses square section 4130 chromoly tubing to simplify the assembly process and improve cost efficiency. The bodywork is designed in multiple sections to keep repair costs low. The bodywork, inspired by a GT car concept and designed by Michael Young, is

manufactured using a five-axis CNC router, which RUSH acquired and refurbished to produce the necessary patterns in-house.

1.3   RUSH SR Vehicle and Gas Motor Parameters

For the following analyses, the constants defined in Table 1.1 were utilized for all computations.

Table 1.1: RUSH SR Vehicle Motor Parameters

Parameter	Symbol	Value	Units
Vehicle Mass	M_V	513	Kilogram [kg]
Driver Mass	M_D	80	Kilogram [kg]
Vehicle Width	w_V	1,500	Millimeter [mm]
Vehicle Height	h_V	990	Millimeter [mm]
Vehicle Length	l_V	3,325	Millimeter [mm]
Gas Power at the Wheels	P_{Gas}	145	Horsepower at Wheel [Hp]
Peak Gas Motor RPM	$\omega_{\text{Gas}}^{\text{Motor}}$	11,800	Revolutions per Minute [RPM]
Front Wheel Radius	r_{Front}	276	Millimeter [mm]
Rear Wheel Radius	r_{Rear}	288	Millimeter [mm]

1.4   Goals of the Project

As with most engineering undertakings involving high-performance sportscars, the goal of this project is to improve the performance of the RUSH SR car. By designing and integrating a hybrid powertrain system into the car, we aim to improve performance in a number of ways, discussed in more detail below.

1.4.1   Increase the Power of the Vehicle

One of the primary goals of adding a hybrid powertrain to the RUSH SR is to increase the overall power output of the vehicle. By combining the vehicle's S-1000 1-Liter Inline Four engine (sourced from a Suzuki GSXS-1000 motorcycle) with an electric motor, we can leverage the strengths of both power sources.

The electric motor can provide instantaneous torque, which is particularly beneficial for

acceleration, while the ICE can deliver sustained power for higher speeds. This hybrid combination can lead to a significant boost in total horsepower and torque, enhancing the car's performance on both straights and corners. Additionally, the hybrid system allows for regenerative braking, which can recover energy that would otherwise be lost, further improving efficiency and performance. Regenerative braking is discussed extensively in chapter 2.

1.4.2 Modifications Should Be Add-Ons, Not Fundamental Changes

RUSH is hoping to sell this hybrid system to existing customers as an add-on. Therefore, the hybrid system must be designed as a modular add-on rather than requiring fundamental changes to the vehicle's architecture. This means that the hybrid components, including the electric motor, battery pack, and associated electronics, should be designed to fit within the existing framework of the RUSH SR. The benefit of this approach is that it allows current RUSH SR owners to upgrade their vehicles without needing to purchase an entirely new car. This modularity can also make maintenance and potential future upgrades simpler and more cost-effective. Ensuring the add-on nature of the hybrid system will be crucial in maintaining customer satisfaction and marketability.

This is a significant constraint on the hybrid system's design and potential capabilities. Ensuring that this system can be retrofitted into a car that was originally designed for internal combustion means that available space is very limited.

1.4.3 Minimize the Additional Weight to the Vehicle

Adding a hybrid powertrain inevitably increases the weight of the vehicle due to the additional components such as the battery pack, electric motor, and power electronics. However, it is crucial to minimize this added weight to preserve the performance characteristics of the RUSH SR. Or, this additional weight should be compensated by the added power from the hybrid components.

Increased weight can negatively impact acceleration, handling, and braking performance. To mitigate these effects, we must focus on using lightweight materials where possible, optimizing the design of the hybrid components, and add mass strategically to ensure that performance is still preserved and improved. Strategically placing the battery and motor to maintain the car's weight distribution will help preserve the vehicle's agility and driving dynamics.

1.4.4 Minimize Hybrid System Cost

While improving performance is a key goal, it is equally important to keep the cost of the hybrid system within a reasonable range. High costs can deter potential customers from opting for the hybrid upgrade, and the entire philosophy of the RUSH SR is to make incredible vehicle performance accessible to enthusiasts at an affordable price.

Therefore, we must aim to design a cost-effective hybrid system without compromising on performance or reliability. This involves selecting affordable yet high-quality components, optimizing manufacturing processes, and considering economies of scale in production. By achieving a balance between performance enhancement and cost efficiency, we can make the hybrid system an attractive option for RUSH SR owners.

1.4.5 Improve Vehicle Acceleration

One of the most noticeable benefits of a hybrid powertrain is the improvement in vehicle acceleration. Electric motors are capable of delivering maximum torque from a standstill, providing a significant boost to initial acceleration. This can be particularly advantageous in racing scenarios where quick starts and rapid acceleration out of corners are critical.

By carefully tuning the interaction between the ICE and the electric motor, we can achieve a seamless power delivery that maximizes acceleration performance. Additionally, incorporating regenerative braking can help maintain battery charge, ensuring that the electric motor can consistently contribute to acceleration throughout a race.

1.4.6 Add a Reverse Gear

The RUSH SR's primary engine is harvested from a Suzuki GSXS-1000 motorcycle, and as a result, the vehicle does not currently have a reverse gear. While motorcycles do not really need reverse gears, the omission of this capability is very inconvenient for owners of the RUSH SR. Needless to say, a reverse gear can be highly practical, especially in scenarios such as maneuvering in tight pit areas or recovering from a spin on the track.

Therefore, adding a reverse gear to the RUSH SR is another important goal of this project. By integrating a reverse gear into the hybrid system, we can provide added convenience and functionality without significantly impacting the car's performance. This can be achieved by using the electric motor to provide reverse propulsion, which simplifies the transmission design and utilizes the existing hybrid components.

Chapter 2

Regenerative Braking

This chapter provides a comprehensive overview of regenerative braking, a critical technology in hybrid and electric vehicles designed to enhance energy efficiency and extend driving range. The discussion begins with Section 2.1, which explains the fundamentals of regenerative braking and its benefits, including energy recovery during braking and reduced wear on traditional braking systems. Section 2.2 reviews the mechanics of how regenerative braking operates, highlighting the conversion of kinetic energy into electrical energy by the electric motor. Section 2.3 explores the role of electric motors functioning as generators, underpinned by Faraday's Law of Electromagnetic Induction and Lenz's Law. This section includes detailed subsections on these electromagnetic principles and their application in energy recuperation during braking. Finally, Section 2.4 addresses practical considerations and limitations, such as electrical resistance, thermal management, inductance, mechanical losses, and core losses, which impact the efficiency and performance of regenerative braking systems. Through these sections, the chapter aims to provide a detailed understanding of the mechanisms, principles, and practical challenges associated with regenerative braking in modern vehicles.

2.1   What is Regenerative Braking?

Regenerative braking is a key technology in hybrid and electric vehicles, aimed at improving energy efficiency and extending driving range. This system recovers a portion of the vehicle's kinetic energy during braking and converts it into electrical energy, which is stored in the battery for later use [3]. This process not only enhances the overall energy efficiency of the vehicle but also reduces wear on the traditional friction braking system.

Researchers have found that in frequent braking situations (like stop-and-go traffic in urban settings), regenerative braking systems can recover 30% to 60% of the total energy dissipated by traditional braking [4], [5].

2.2   How Regenerative Braking Works

During the braking process, the electric motor of an electric vehicle can function as an electric generator, converting the vehicle's kinetic or potential energy into electric energy. This electrical energy can then be stored in the battery for later use when the driver accelerates the vehicle in the future [6], [7].

Unlike traditional braking systems that reduce the kinetic energy of a moving vehicle by dissipating mechanical energy into heat through friction between the brake pads and the wheels, regenerative braking systems in vehicles with electric motors reduce the vehicle's kinetic energy by partially converting it into electrical energy through the use of the electric motor as a generator, which then stores this energy in the vehicle's battery [8].

Table 2.1: Energy Consumption During Braking with Regenerative Braking [8].

Energy	Value [Joules]	Percentage [%]
Total Kinetic Energy	4.430×10^5	100%
Rolling Resistance	5.089×10^4	11.49%
Wind Resistance	8.879×10^3	2.00%
Hydraulic Braking	9.290×10^4	20.97%
Regenerative Braking	2.489×10^5	56.19%
Other	4.140×10^4	9.35%

2.3   Electric Motors as Generators

Electric motors and generators operate on the same fundamental principles of electromagnetism. An electric motor can function as a generator when mechanical energy is applied to its rotor, causing it to rotate [9]. This process effectively operates the motor in reverse, converting mechanical energy back into electrical energy [10].

2.3.1   Faraday's Law of Electromagnetic Induction

The fundamental principle governing this process is Faraday's Law of Electromagnetic Induction [11]. According to Faraday's Law, a change in magnetic flux through a coil induces an electromotive force (EMF) in the coil. This relationship is described by the equation:

$$\mathcal{E} = -N\frac{d\Phi}{dt} \tag{2.1}$$

where $\mathcal{E}$ is the induced EMF (voltage), N is the number of turns in the coil, and $\frac{d\Phi}{dt}$ is the rate of change of magnetic flux Φ through the coil. In the context of a motor acting as a generator, the mechanical rotation of the rotor changes the magnetic flux through the stator windings, thereby inducing a voltage [12]–[14].

2.3.2 Lenz's Law

Lenz's Law [15] is a fundamental principle in electromagnetism that describes the *direction* of the induced EMF and current resulting from a change in magnetic flux $\frac{d\Phi}{dt}$. It is intrinsically linked to Faraday's Law of Electromagnetic Induction (2.1) and provides critical insights into the behavior of electric motors and generators.

The negative sign indicates that the induced EMF ($\mathcal{E}$) generates a current whose magnetic field opposes the original change in magnetic flux ($\frac{d\Phi}{dt}$).

2.3.3 Operation as a Generator

When a motor is powered, electrical energy is supplied to the windings, creating a magnetic field that interacts with the rotor to produce motion. Conversely, if mechanical energy is applied to the rotor, it will rotate within the magnetic field of the stator. This rotation changes the magnetic flux through the windings over time, inducing a voltage according to Faraday's Law (2.1).

The generated voltage V in this scenario can be described by equation (2.2).

$$V = k \cdot \omega \tag{2.2}$$

where V is the generated voltage, k is a constant that depends on the motor's construction (often referred to as the back EMF constant or motor constant), and ω is the angular velocity of the motor (rotor speed). This equation indicates that the voltage generated by the motor when used as a generator is directly proportional to the speed at which the motor is driven.

2.3.4 Energy Recuperation in Regenerative Braking

Faraday's Law of Electromagnetic Induction is a key principle enabling regenerative braking in electric motors. During regenerative braking, the motor operates as a generator. As the vehicle slows down, the wheels drive the motor, causing the rotor to rotate and altering the magnetic flux (Φ) through the stator windings. This change in magnetic flux ($\frac{d\Phi}{dt}$) induces an EMF ($\mathcal{E}$), which drives a current through the motor windings. The direction of this current

is such that it opposes the motion of the rotor, providing a braking force to the vehicle in accordance with Lenz's Law, as discussed in section 2.3.2. The electrical energy generated is then fed back into the vehicle's battery or energy storage system, recuperating some of the kinetic energy that would otherwise be lost as heat during conventional braking [16].

The implications of Faraday's Law for regenerative braking are profound. By converting kinetic energy back into electrical energy, regenerative braking significantly enhances the overall efficiency of the vehicle, reducing energy waste and extending the vehicle's range on a single charge [17]. Furthermore, the improved energy efficiency resulting from regenerative braking contributes to lower energy consumption and reduced emissions, aligning with environmental sustainability goals [18]. In the context of the RUSH SR racecar, this improved efficiency enables the size of the battery to be reduced as it can be assumed that a portion of the energy expended during acceleration could be recaptured during decelleration through regenerative braking.

2.4 Practical Considerations and Limitations

In practical applications, several factors influence the efficiency and performance of a motor used as a generator.

2.4.1 Resistance

Electrical resistance in the windings is a significant factor that affects the efficiency of a generator. Resistance causes energy losses in the form of heat, which reduces the overall output voltage and power. These resistive losses are governed by Joule's Law [19], which states that the power loss due to resistance is proportional to the square of the current flowing through the windings:

$$P = I^2 R$$

where P is power, I is the current, and R is the resistance of the wire. This equation indicates that even small increases in current can lead to significant increases in power loss due to heat, as the power loss scales with the square of the current.

In the context of using a motor as a generator, this implies that the resistive losses can become substantial, particularly at higher currents. Therefore, minimizing resistance through the use of high-quality conductive materials, such as copper or silver, and employing efficient winding techniques is crucial for improving the performance of the motor as a generator. By reducing resistance, the generator can operate more efficiently, converting a greater proportion of the mechanical energy into electrical energy while minimizing energy losses in the form of heat.

2.4.2 Thermal Management

The opposition created by the induced EMF ($\mathcal{E}$) according to Lenz's Law can generate heat due to resistive losses in the motor windings. Effective thermal management is crucial to ensure that this heat does not adversely affect the motor's performance and longevity. By minimizing resistive losses through high-quality materials and efficient cooling systems, the negative impact of heat generation can be mitigated, ensuring optimal performance of the motor both as a motor and a generator [20].

2.4.3 Inductance

The inductive properties of the windings can influence the voltage and current characteristics of the generator, especially under varying load conditions. Inductance causes a phase shift between the current and voltage, which can lead to reactive power losses and reduce the real power output. In addition, the inductance of the windings can cause transient effects and voltage spikes when there are sudden changes in load. Designing the windings to have appropriate inductance values and using proper filtering techniques can help mitigate these effects.

2.4.4 Mechanical Losses

Mechanical losses, such as friction in the bearings and air resistance against the rotor, also impact the efficiency of the generator. These losses convert some of the mechanical energy applied to the rotor into heat, reducing the amount of energy available for conversion to electrical energy. High-quality bearings and lubrication can reduce frictional losses, while aerodynamic design of the rotor can minimize air resistance. Ensuring that the mechanical components are well-maintained is essential for maintaining high efficiency in the energy conversion process.

2.4.5 Core Losses

Magnetic core losses, which include hysteresis and eddy current losses, occur in the stator core as it undergoes cyclic magnetization. Hysteresis losses are due to the lag between the magnetizing force and the magnetic flux density, while eddy current losses are caused by circulating currents induced in the core material. These losses result in additional heating of the core, further reducing the efficiency of the generator. Using high-quality core materials with low hysteresis and electrical resistivity, such as laminated silicon steel, can help minimize these losses.

Chapter 3

Vehicle Race Data Analysis

This chapter discusses the analysis of race data collected from the RUSH SR vehicle to explore the potential benefits and performance implications of regenerative braking systems in competitive racing. Following the foundational concepts outlined in Chapter 2, this chapter evaluates how regenerative braking can enhance the RUSH SR's energy efficiency, acceleration, and overall race performance. The analysis is structured into several key sections: Section 3.1 discusses the implications of regenerative braking for the RUSH SR, highlighting its potential impact on energy recovery, acceleration, and braking efficiency. Section 3.2 introduces the race tracks—Palmer Motorsports Park and the Podium Club Racetrack—providing context for the collected race data. The subsequent sections, 3.4, 3.5, and 3.6, present detailed analyses of vehicle velocity, throttle usage, and longitudinal acceleration during races, respectively. Finally, Section 3.7 offers insights into braking patterns and pressures, crucial for understanding the regenerative braking system's effectiveness. Together, these sections provide a comprehensive view of how regenerative braking can be optimized to enhance hybrid vehicle performance in motorsports.

3.1 Implications of Regenerative Braking for the RUSH SR

Regenerative braking systems increase the overall energy efficiency of the vehicle by converting kinetic energy, typically lost as heat during braking, into electrical energy using the principles of Faraday's Law of Electromagnetic Induction (2.1), as described in greater detail in section 2.3. This recovered energy is stored in batteries or supercapacitors and can be reused to power the car, thus extending its operational range. This increased range can reduce the frequency of pit stops or battery swaps, providing a strategic advantage in endurance races.

In terms of performance, regenerative braking systems contribute to enhanced acceleration

by allowing the stored energy to be used as an additional power boost during critical moments, such as overtaking maneuvers or acceleration after heavy braking during cornering. Moreover, the integration of these systems can improve the car's weight distribution by strategically placing the batteries and related components, thereby enhancing handling and stability. This dual benefit of improved acceleration and better handling can significantly impact the car's lap times and overall race performance.

The efficiency of the braking system itself is also markedly improved with the inclusion of regenerative braking. The reduced reliance on mechanical brakes decreases the wear and tear on brake components, extending their lifespan and ensuring consistent braking performance throughout the race. Additionally, by converting a portion of the braking energy into electrical energy, less heat is generated in the brake discs and pads, which mitigates the risk of brake fade during extended racing sessions. This improvement in heat management is crucial for maintaining optimal braking performance under the high-stress conditions of competitive racing.

Strategically, regenerative braking systems provide teams with greater flexibility in energy management. The ability to store and deploy energy tactically can offer significant advantages, such as in drag reduction systems (DRS) zones or during high-demand sections of the track. Additionally, regenerative braking systems can be fine-tuned to adapt to various track conditions and driving styles, offering drivers enhanced control and responsiveness.

The following chapter will provide an in-depth analysis of how regenerative braking could be utilized in the RUSH SR, anticipated energy gains from such a system, as well as a discussion of how an energy recuperation system could reduce the size of the hybrid vehicle's battery.

3.2   Race Tracks

RUSH Auto Works provided race data for multiple races and tests at two different race tracks. Palmer Motorsports Park located in Palmer, Massachusetts, discussed in greater detail in section 3.2.1. The engineers at RUSH also provided track data for multiple tests at the Podium Club Racetrack located in Casa Grande, Arizona, discussed in greater detail in section 3.2.2.

3.2.1   Palmer Motorsports Park

Palmer Motorsports Park, situated on Whiskey Hill in Hampden County, Massachusetts, is a motorsports venue that offers a thrilling experience for racing enthusiasts. Located at 58 W Ware Road, Palmer, Massachusetts, the track is only a 1.5 hour drive from MIT's campus. Officially opened in May 2015, the park features the Whiskey Hill Raceway, a 2.3-mile road course that features 190 feet of elevation change and 14 turns [21]. This technical track is

known for its challenging layout and significant elevation changes, making it a favorite among drivers seeking to test their skills and companies looking to collect data on the performance of their vehicles. A satellite map of the racetrack can be viewed in figure 3.1.
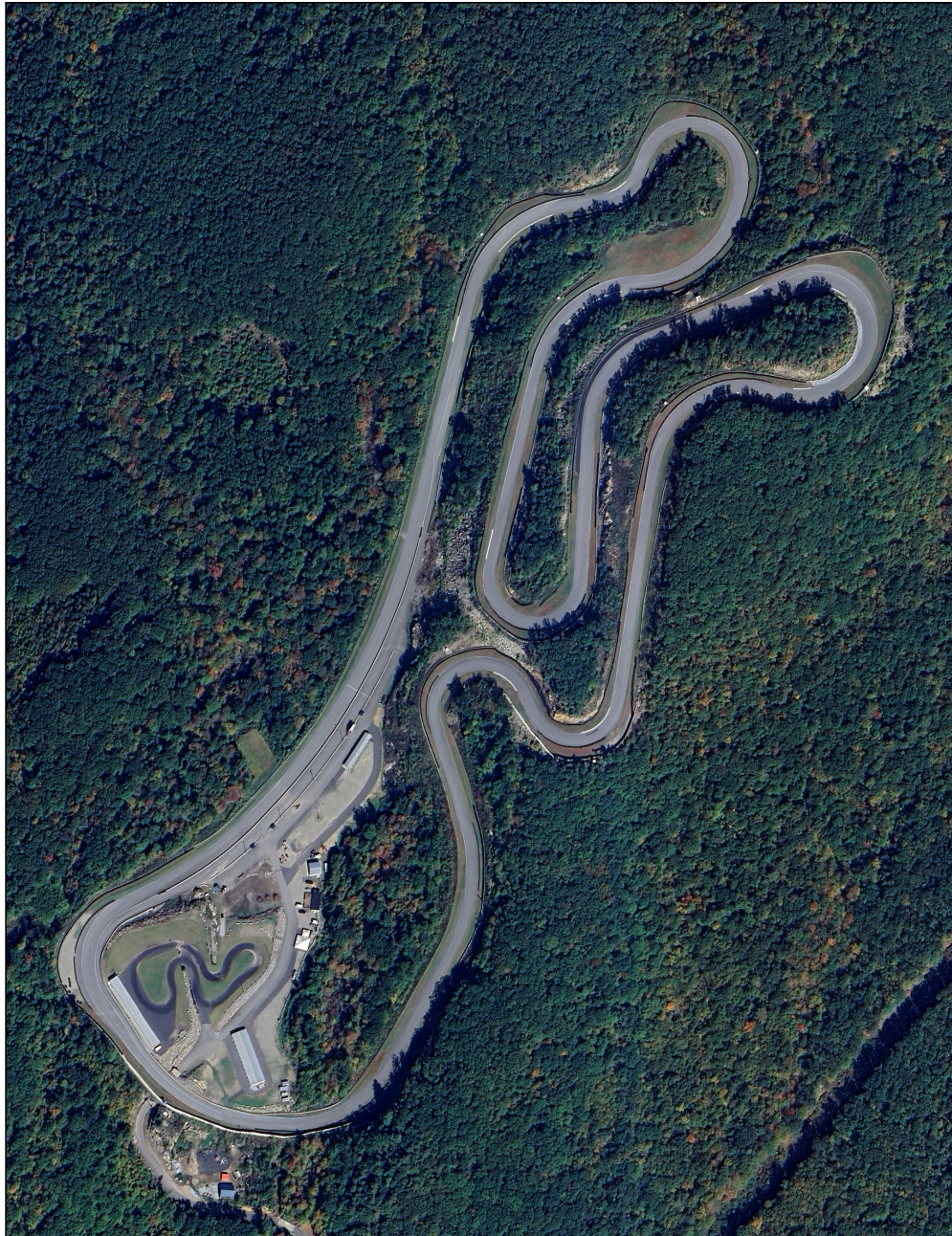
Figure 3.1: Satellite Map of Palmer Motorsports Park in Palmer, Massachusetts

The creation of Palmer Motorsports Park stemmed from the New England Region (NER) of the Sports Car Club of America's need for a local and cost-effective racing venue. Following the initial approval in 2007, the project faced delays but was revitalized in 2014 by SCCA members Fred Ferguson and Jonathan Fryer, who completed the track's construction in 2015 [22]. The track is used extensively for club racing, driver training, and various motorsports

events, running approximately 32 weeks a year from April to November.

Palmer Motorsports Park is praised for its design, which combines speed with technical corners and dramatic elevation changes that challenge drivers' courage and skill. The track can be run in both clockwise and counter-clockwise directions, thanks to safety modifications implemented in 2017. This being said, all analyses performed for this study were conducted in the counter-clockwise direction.

Despite some challenges, Palmer Motorsports Park has gained recognition as one of the top racetracks to drive in North America, offering a unique and exhilarating motorsports experience in the heart of New England.

3.2.2 Podium Club Racetrack

Figure 3.2: Satellite Map of the Podium Club Racetrack in Casa Grande, Arizona

The Podium Club at Attesa, located in Arizona, features a 2.32-mile, 15-turn road course designed to test drivers' abilities. This versatile track offers 18 different configurations, allowing for simultaneous operation of two tracks [23]. The circuit includes generous runoff areas, large gravel traps, challenging elevation changes, and a high-speed front straight. Engineered by Apex Circuit Design, it employs energy-absorbing hydro barriers for maximum

safety. The track width ranges from 40 to 50 feet, and it accommodates noise levels up to 120 dB, making it suitable for various racing events. A satellite map of the racetrack can be viewed in figure 3.2.

Located at 6870 S Bianco Road, Casa Grande, Arizona, the Podium Club at Attessa is a frequent testing facility used by RUSH Auto Works to test different configurations of the vehicle and different driving conditions.

3.3 Analyzing Race Data

To assist with the data analysis, performance estimations, and vehicle simulations, RUSH Auto Works provided us with high-quality track data for this project. Track data collected at Palmer Motorsports Park and the Podium Club Racetrack will be utilized and compared in this analysis.

3.4 Vehicle Velocity Analysis During Races

To accurately estimate the theoretical energy recuperation capabilities of a regenerative braking system, the vehicle's kinetic energy throughout a lap of a race must be identified. As such, the velocity profile of the RUSH SR is reviewed and analyzed.

The RUSH SR's speed plots for a given lap at the Palmer Motorsports Park and the Podium Club Racetrack, offer a detailed representation of vehicle dynamics throughout a single lap on each track. These plots, which display vehicle speed in miles per hour, highlight the variability and fluctuations in speed as the vehicle navigates different sections of the tracks.

At Palmer Motorsports Park, the vehicle's speed oscillates between approximately 43.73 mph and 123.29 mph, as depicted in Figure 3.3. The average speed achieved during this race was 75.53 MPH, and the standard deviation of the vehicle's velocity was 21.23 MPH during this lap, as highlighted in Table 3.1.

This variation in speed is indicative of the diverse nature of the racetrack, which includes a combination of straight sections, curves, and sharp turns. The lower speeds are observed at tight corners and sharp turns where the vehicle must decelerate significantly, while the higher speeds occur in the straighter sections of the track where the driver can accelerate. The pattern of acceleration and deceleration, marked by peaks and valleys in the plot, is typical of racing, emphasizing the necessity of maintaining high speeds on straight sections and careful braking into turns. Specific points with abrupt changes in speed likely indicate critical sections of the track, such as hairpin turns or chicanes, which demand sudden deceleration and precise maneuvering.
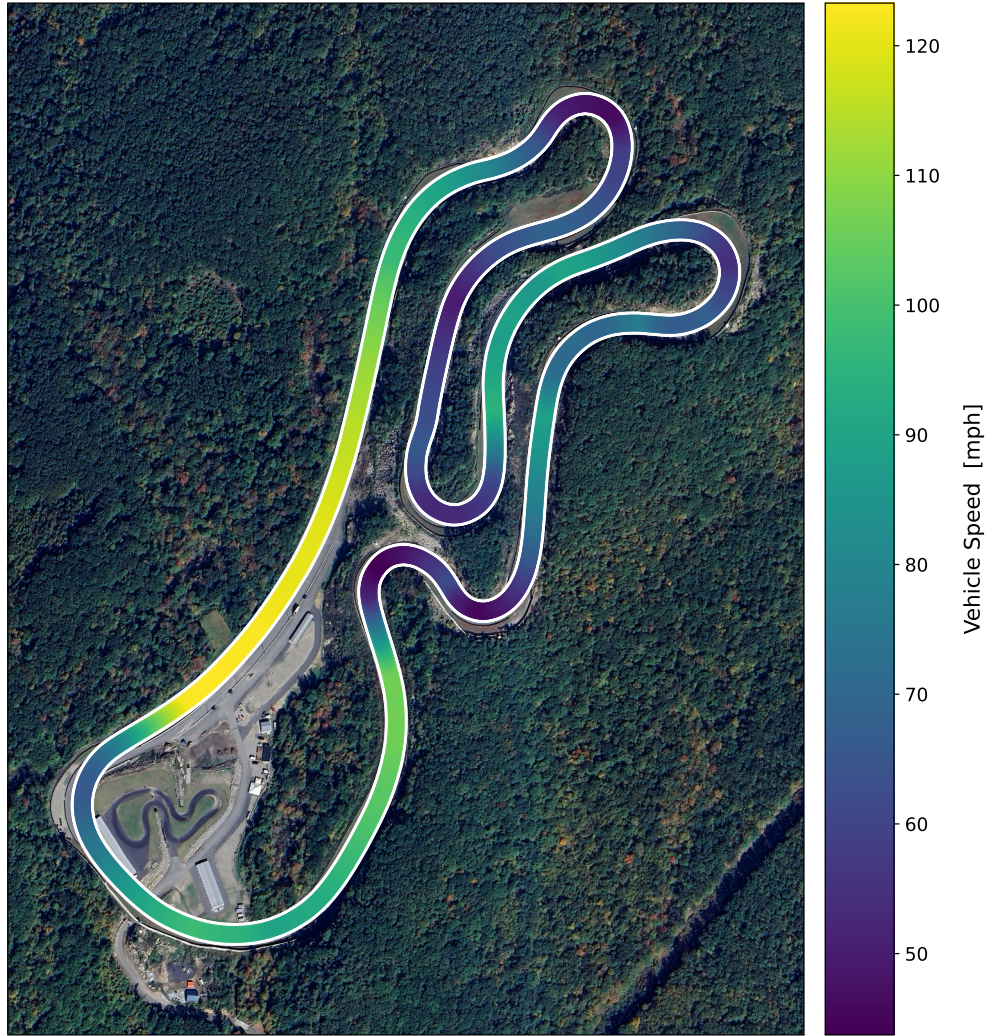
Figure 3.3: RUSH SR Vehicle Speed for a Lap at the Palmer Motorsports Park

Similarly, the RUSH SR's velocity at the Podium Club Racetrack, as depicted in Figure 3.4, illustrates vehicle speeds ranging from about 50 mph to 120 mph. The average speed achieved during this race was 80.33 MPH, and the standard deviation of the vehicle's velocity was 19.67 MPH during this lap, as highlighted in Table 3.1.

The pattern of speed variability, while similar in range to the Palmer track, exhibits differences that suggest unique characteristics of the Podium track, such as more prolonged straightaways and different configurations of turns. The plot's clear peaks (high-speed yellow zones) and valleys (low-speed purple zones) reflect the vehicle's performance as it navigates various sections of the track. The distribution and frequency of speed changes provide insights into the track's complexity, with more frequent speed changes potentially indicating a track with numerous turns and fewer straight sections.

The statistical data presented in Table 3.1 provides further insights into the vehicle's per-
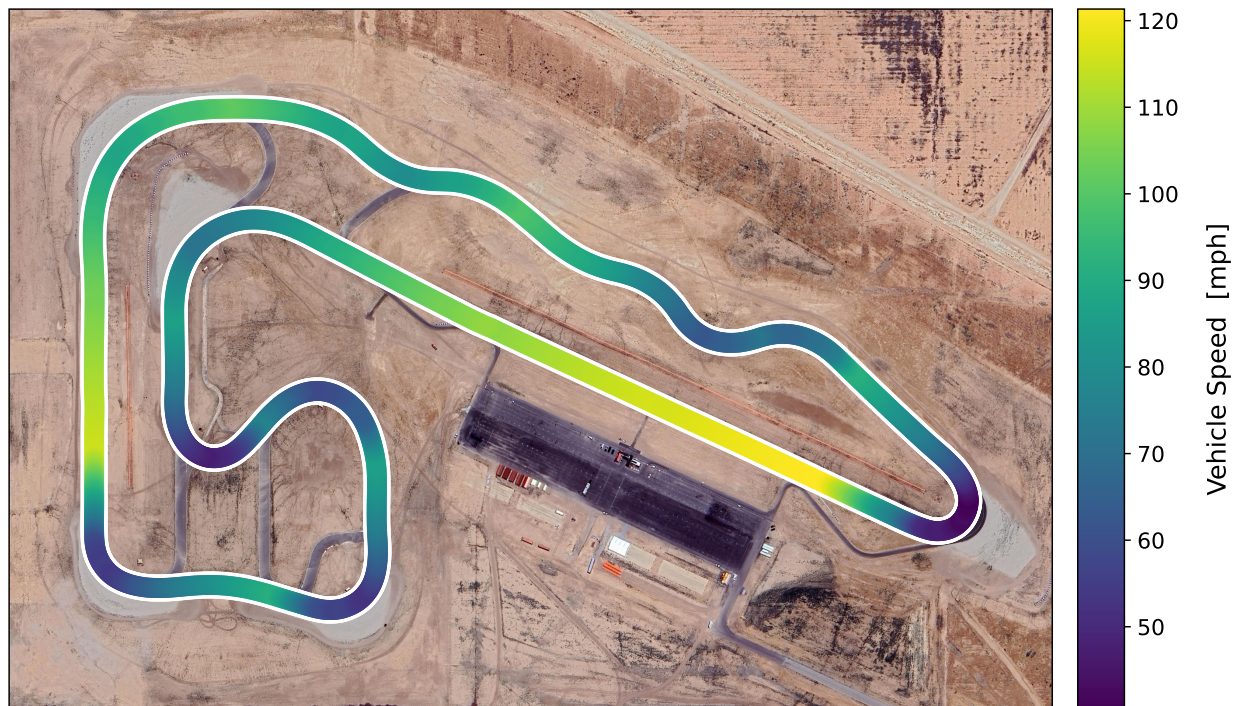
Figure 3.4: RUSH SR Vehicle Speed for a Lap at the Podium Club Racetrack

formance on each track. At Palmer Motorsports Park, the average speed was 75.53 MPH with a standard deviation of 21.23 MPH, indicating substantial variability in speed due to the track's diverse layout. The maximum speed recorded was 123.29 MPH, while the minimum was 43.73 MPH. These differences in velocity highlight the vehicle's need to decelerate significantly at certain points, which is crucial for understanding the potential energy recuperation through a regenerative braking system. The wide range of speeds and significant deceleration events suggest numerous opportunities for energy recovery during braking.

In contrast, at the Podium Club Racetrack, the average speed was slightly higher at 80.33 mph, with a lower standard deviation of 19.67 mph. The maximum and minimum speeds were 121.34 mph and 40.44 mph, respectively. The higher average speed and slightly lower variability suggest a track layout with more prolonged straightaways and fewer sharp turns, which might result in fewer but potentially more significant deceleration events. This pattern implies different energy recuperation dynamics compared to the Palmer track, potentially affecting the design and efficiency of the regenerative braking system.

Comparing both plots 3.3 and 3.4 reveals insights into the distinct characteristics of each track. Both tracks have sections requiring significant braking and acceleration, but the nature and frequency of these sections differ, indicating the varied design and difficulty levels of the tracks. Additionally, these plots reflect the driver's ability to handle the vehicle, showing their skill in accelerating on straights and controlling the car through turns. Consistent patterns of speed changes suggest a good rhythm and a strong understanding of the track layout. Furthermore, the vehicle's capability to quickly accelerate and decelerate is highlighted in

Table 3.1: RUSH SR Velocity Statistics (in MPH) at Palmer Motorsports Park and the Podium Club Racetrack

Velocity [MPH]	Palmer Motorsports Park	Podium Club Racetrack
Mean	75.53	80.33
Standard Deviation	21.23	19.67
Minimum	43.73	40.44
5th Percentile	47.54	48.93
10th Percentile	50.56	54.83
25th Percentile	58.45	65.23
Median (50th Percentile)	70.33	80.12
75th Percentile	90.87	93.61
90th Percentile	106.14	109.27
95th Percentile	118.69	115.09
Maximum	123.29	121.34

these plots, with maximum speeds and rates of deceleration providing insights into the car's performance characteristics. Vehicle acceleration statistics and plots are discussed later in section 3.6.
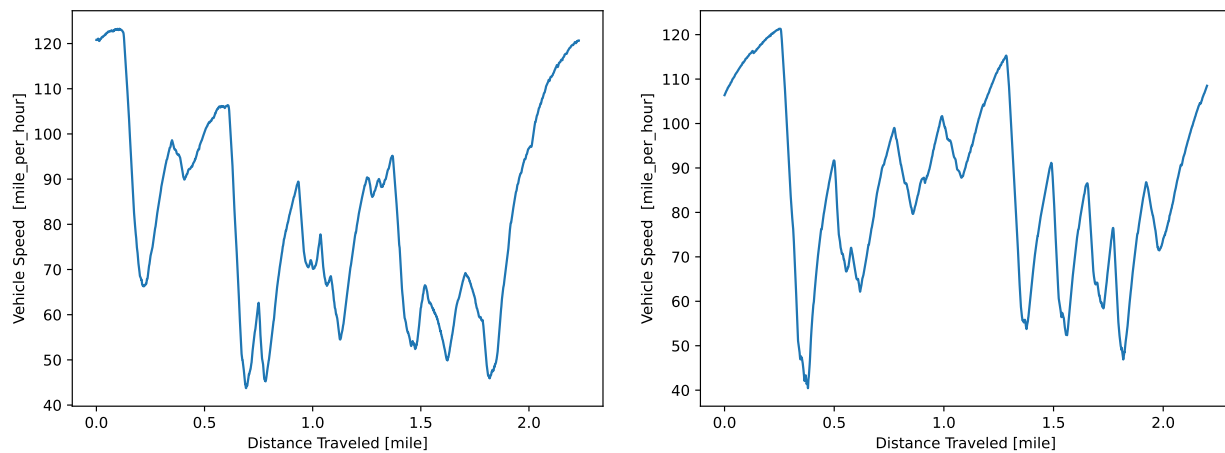
(a) Velocity at Palmer Motorsports Park   (b) Velocity at the Podium Club Racetrack

Figure 3.5: Individual RUSH SR Velocity graphs: (a) Velocity of a Lap at Palmer Motorsports Park; (b) Velocity of a Lap at the Podium Club Racetrack.

Figure 3.5 highlights the vehicle velocity for a single lap across distance in a more traditional format. Figure 3.5a details this data for Palmer, and Figure 3.5b details this data for the Podium Club. This representation allows for a clear visualization of how the vehicle's speed changes at specific points along the track. By plotting speed against distance, it becomes easier to identify sections where the vehicle accelerates and decelerates, which correspond to

straightaways and corners, respectively. This traditional format aids in pinpointing critical areas of the track that demand the most from the vehicle's braking system, providing valuable insights for optimizing the regenerative braking system. For example, areas with frequent or significant deceleration events represent prime opportunities for energy recuperation.

(a) Velocity at Palmer Motorsports Park

(b) Velocity at the Podium Club Racetrack
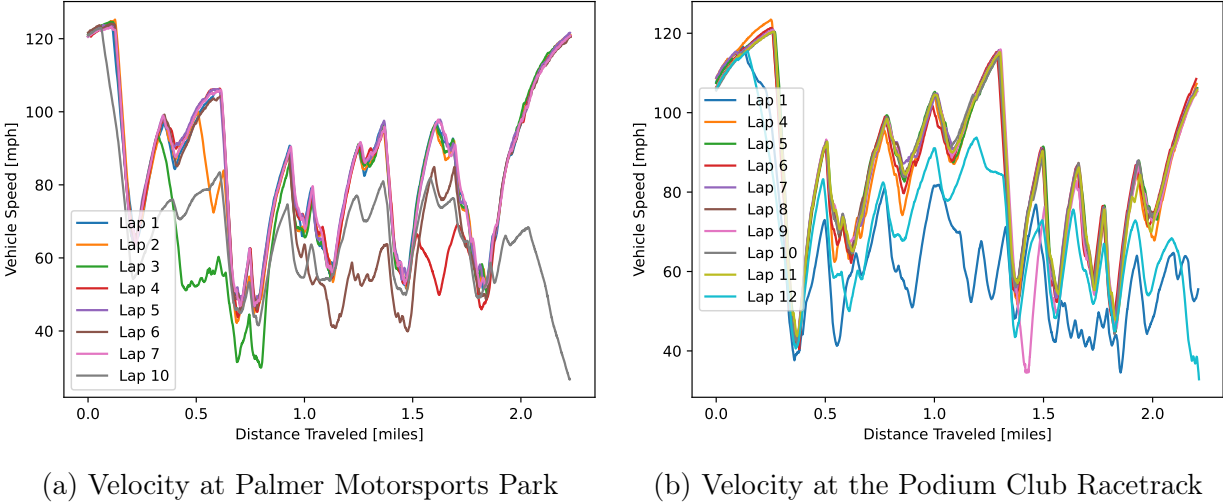
Figure 3.6: RUSH SR Velocity Graphs for All Laps During a Race: (a) Velocity of Laps at Palmer Motorsports Park; (b) Velocity of Laps at the Podium Club Racetrack.

Likewise, Figure 3.6 highlights the vehicle's velocities for each lap. Figure 3.6a details this data for Palmer, and Figure 3.6b details this data for the Podium Club. This comprehensive view across multiple laps allows for the analysis of consistency and performance trends over time. By examining the speed data across all laps, we can assess the driver's consistency in handling the vehicle and the track. Analyzing the velocities across multiple laps can help in understanding the long-term implications for the regenerative braking system. Repeated patterns of deceleration across laps can indicate sustained opportunities for energy recovery, while variations might suggest areas where system adjustments could enhance performance. Overall, these insights are crucial for developing a robust and efficient regenerative braking system tailored to the vehicle's racing dynamics.

In conclusion, the analysis of vehicle speed plots for the Palmer and Podium racetracks provides a comprehensive view of vehicle dynamics over the course of a lap on each track. These plots, along with the detailed statistical data, offer valuable insights into driver skill and vehicle performance, which are critical factors in competitive racing. Additionally, the implications for a regenerative braking system are significant, as the varied speed profiles and deceleration events on each track highlight different opportunities and challenges for energy recuperation. Understanding these dynamics is essential for optimizing the regenerative braking system's design and effectiveness.

3.5 Throttle Usage Analysis During Races

Throttle usage throughout a race provides critical insights into the nature of how the vehicle is being operated by the driver, as well as how aggressively the driver is attempting to accelerate the vehicle. Detailed examination of the throttle behavior across these tracks offers insights into how different driving conditions and track layouts influence potential energy recovery and vehicle efficiency.
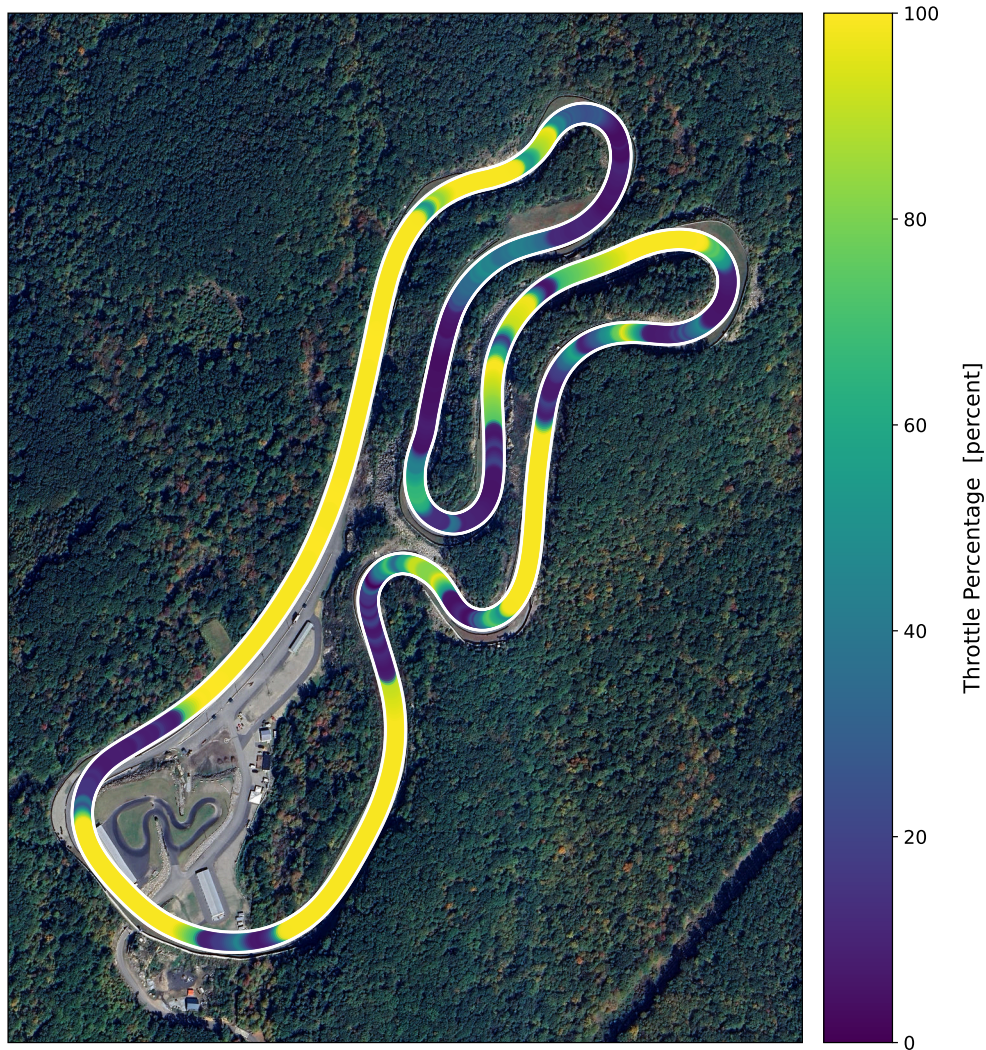
Figure 3.7: RUSH SR Throttle Percentage for a Lap at Palmer Motorsports Park

In the Palmer racetrack plot, depicted in Figure 3.7, the throttle percentage ranges from 0% (no throttle usage whatsoever) to 100% (the throttle is being floored). This data represents the throttle usage over the course of a single lap. Significant variation in throttle usage is observed throughout the lap, indicating that the driver adjusts the throttle in response to the track's layout, which includes straightaways, curves, and braking zones. High throttle sections, where the percentage approaches or reaches the maximum value, suggest areas of

the track where the vehicle is accelerating on straight paths. Conversely, low throttle sections indicate zones where the vehicle is decelerating, potentially employing the regenerative braking system to recover energy.
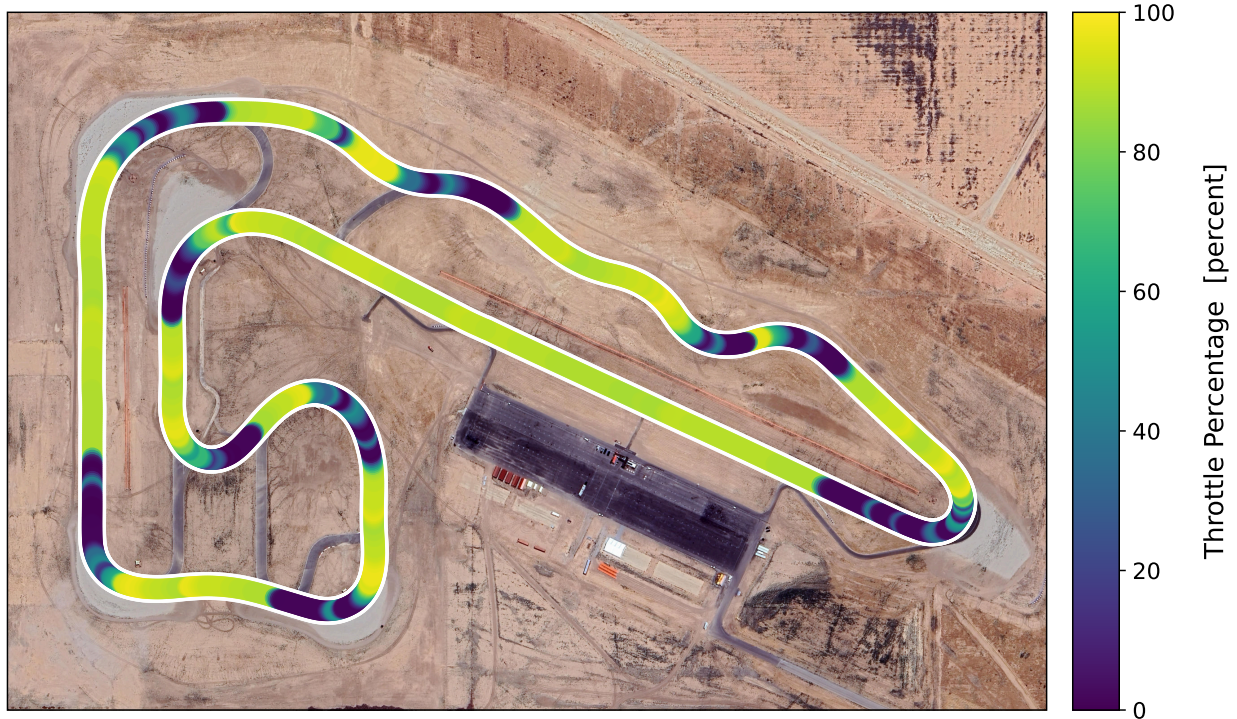
Figure 3.8: RUSH SR Throttle Percentage for a Lap at the Podium Club Racetrack

Similarly, the Podium racetrack plot, depicted in Figure 3.8, demonstrates that the throttle percentage ranges from 0% (no throttle usage whatsoever) to 100% (the throttle is being floored). The dynamic changes in throttle usage reflect the driver's input to navigate the track efficiently, highlighting frequent adjustments. High throttle percentages correspond to acceleration phases, while lower percentages indicate deceleration phases where regenerative braking might be active. A comparison of throttle usage patterns between Palmer and Podium racetracks provides insights into how different track layouts influence the usage and effectiveness of the regenerative braking system.

By analyzing these throttle usage plots and the accompanying statistics in Table 3.2, several aspects regarding the regenerative braking system can be inferred. The mean throttle usage at Palmer Motorsports Park is 54.99%, while at the Podium Club Racetrack, it is higher at 60.96%. This indicates that the vehicle spends less time accelerating at Palmer compared to Podium.

A lower mean throttle percentage would be indicative of more frequent periods of braking or coasting. The standard deviations of 39.32% for Palmer and 37.34% for Podium indicate considerable variability in throttle usage, reflecting the dynamic nature of driving on these tracks. The median throttle usage values, however, reveal a stark contrast, with Palmer at

Table 3.2: RUSH SR Throttle Percent Statistics (in %) at Palmer Motorsports Park and the Podium Club Racetrack

Throttle Usage [%]	Palmer Motorsports Park	Podium Club Racetrack
Mean	54.99	60.96
Standard Deviation	39.32	37.34
Minimum	0.0	0.0
5th Percentile	5.31	1.20
10th Percentile	6.19	1.20
25th Percentile	10.62	21.69
Median (50th Percentile)	53.98	87.95
75th Percentile	99.12	90.36
90th Percentile	99.12	92.77
95th Percentile	99.12	96.39
Maximum	100.00	100.00

53.98% and Podium at a much higher 87.95%. These differences provide crucial insights into the driving dynamics and the effectiveness of the regenerative braking system in hybrid vehicles under varied track conditions, and are discussed in further detail in Section 3.5.1.

In terms of the implications on energy recovery during a race, the analysis of throttle usage statistics from the Palmer and Podium racetracks provides valuable insights into the driving dynamics and the potential effectiveness of the regenerative braking system in hybrid vehicles. By understanding how different track layouts influence throttle usage, we can better evaluate and optimize the regenerative braking strategies to enhance energy recovery and vehicle efficiency. A track with more frequent periods of strong deceleration would be able to recharge the vehicle's battery throughout the race, whereas a track with fewer corners and longer straightaways would result in an energy recovery profile that is more sporadic, but with greater overall magnitude. In other words, tracks with frequent braking zones like Palmer offer more consistent opportunities for energy recovery, while tracks with sustained high throttle like Podium may require strategic utilization of brief braking periods to maximize the benefits of regenerative braking.

3.5.1 Mean vs. Median Throttle Usage

As highlighted in Table 3.2, the mean throttle usage at Palmer Motorsports Park is 54.99%, whereas at the Podium Club Racetrack, it is slightly higher at 60.96%. This suggests that, on average, the vehicle spends more time accelerating or applying higher throttle at Podium than at Palmer. This could also suggest that, on average, the vehicle spends more time coasting or decelerating at Palmer. It should be noted that the mean value provides a

general sense of the overall throttle usage but can be influenced by extreme values, such as periods of full throttle or no throttle.

Notably, the median throttle usage reveals a stark contrast, with Palmer at 53.98% and Podium at a significantly higher 87.95%. The median value, representing the middle point of the data distribution, indicates that more than half of the throttle usage at Podium is above 87.95%, suggesting a more aggressive or consistent throttle application. This high median compared to the mean implies that the throttle usage at Podium is skewed towards higher values, likely because the track enables longer and more sustained acceleration periods or has fewer low-speed segments compared to Palmer. This hypothesis is confirmed by reviewing the vehicle velocity graphs in Figures 3.3 and 3.4, showing that there are more and longer straightaways that allow the RUSH SR to reach higher velocities.

(a) Palmer Motorsports Park (b) Podium Club Racetrack
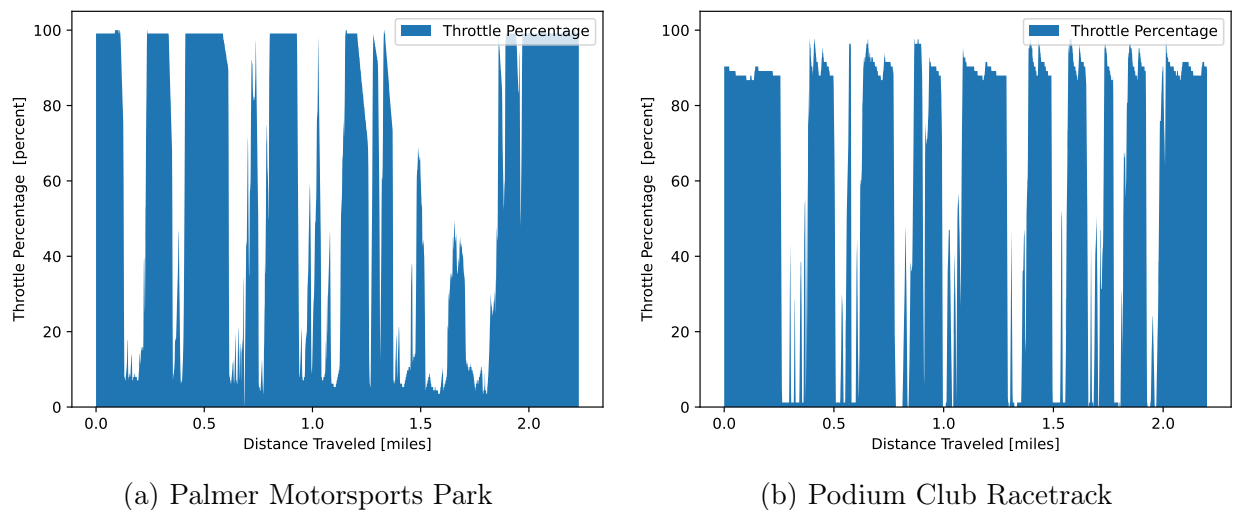
Figure 3.9: RUSH SR Throttle Usage: (a) Throttle Usage of a Lap at Palmer Motorsports Park; (b) Throttle Usage of a Lap at the Podium Club Racetrack.

The disparity between the mean and median throttle values at Podium, where the median is significantly higher than the mean, suggests that there are frequent periods where the throttle is applied near its maximum, interspersed with very few instances of low throttle usage. This pattern is illustrated in Figure 3.9, which compares throttle usage across different tracks. This pattern is consistent with tracks that feature long straightaways or fewer braking zones, allowing the driver to maintain higher throttle for extended periods.

On the other hand, Palmer shows a more balanced throttle application with a mean and median that are close, suggesting a more evenly distributed throttle usage throughout the lap. This distribution indicates that Palmer has a mix of high-speed and low-speed segments, requiring the driver to frequently adjust the throttle, reflecting a track with a combination of straights and technical sections.

The percentile statistics further clarify the throttle usage patterns. At Podium, the lower percentiles (5th and 10th) show very low throttle usage, around 1.20%, indicating brief but very low throttle applications, likely in sharp corners or hairpin turns. However, the 25th

percentile jumps significantly to 21.69%, showing that even the lower quartile of throttle usage at Podium is relatively high, reinforcing the idea of sustained throttle application during most of the lap.

At Palmer, the lower percentiles (5th and 10th) are higher than those at Podium (5.31% and 6.19%), suggesting more frequent use of moderate throttle levels rather than extremes. This reflects a track that demands more variable throttle control, likely due to a more intricate layout requiring more precise handling and varied acceleration and deceleration phases.

The higher percentiles (75th, 90th, and 95th) at Podium are consistently higher than those at Palmer, indicating that Podium generally requires more aggressive throttle usage for a significant portion of the lap. The high values in these percentiles suggest extended periods of near-maximum throttle application, further supporting the idea that Podium has fewer low-speed sections and more opportunities for full throttle acceleration.

Understanding these statistics is crucial for evaluating the regenerative braking system. Tracks like Podium, which require sustained high throttle and have fewer low-speed sections, may present fewer opportunities for regenerative braking, as energy recovery primarily occurs during deceleration phases. However, the few instances of low throttle usage at Podium, reflected in the lower percentiles, could be key moments where significant energy recovery is possible if regenerative braking is effectively utilized during these brief deceleration phases.

At Palmer, with its more balanced throttle application and frequent moderate to high deceleration phases, there are more opportunities for regenerative braking. The regenerative system can be optimized to recover energy efficiently during these frequent transitions between acceleration and deceleration.

Overall, the analysis of throttle usage statistics from the Palmer and Podium racetracks provides valuable insights into the driving dynamics and the potential effectiveness of the regenerative braking system in hybrid vehicles. By understanding how different track layouts influence throttle usage, we can better evaluate and optimize the regenerative braking strategies to enhance energy recovery, vehicle efficiency, and optimally select the size of the battery. Tracks with frequent braking zones like Palmer offer more consistent opportunities for energy recovery, while tracks with sustained high throttle like Podium may require strategic utilization of brief braking periods to maximize the benefits of regenerative braking.

3.6   Inline Acceleration Analysis During Races

To properly evaluate the energy recuperation capabilities of a hybrid powertrain system during a race, vehicle acceleration data can be used to quantify the magnitude of kinetic energy lost during periods of deceleration. In this section, longitudinal acceleration data for the RUSH SR is analyzed to estimate the amount of energy that could potentially be recuperated throughout a lap of a race. Data from both the Palmer Motorsports Park and
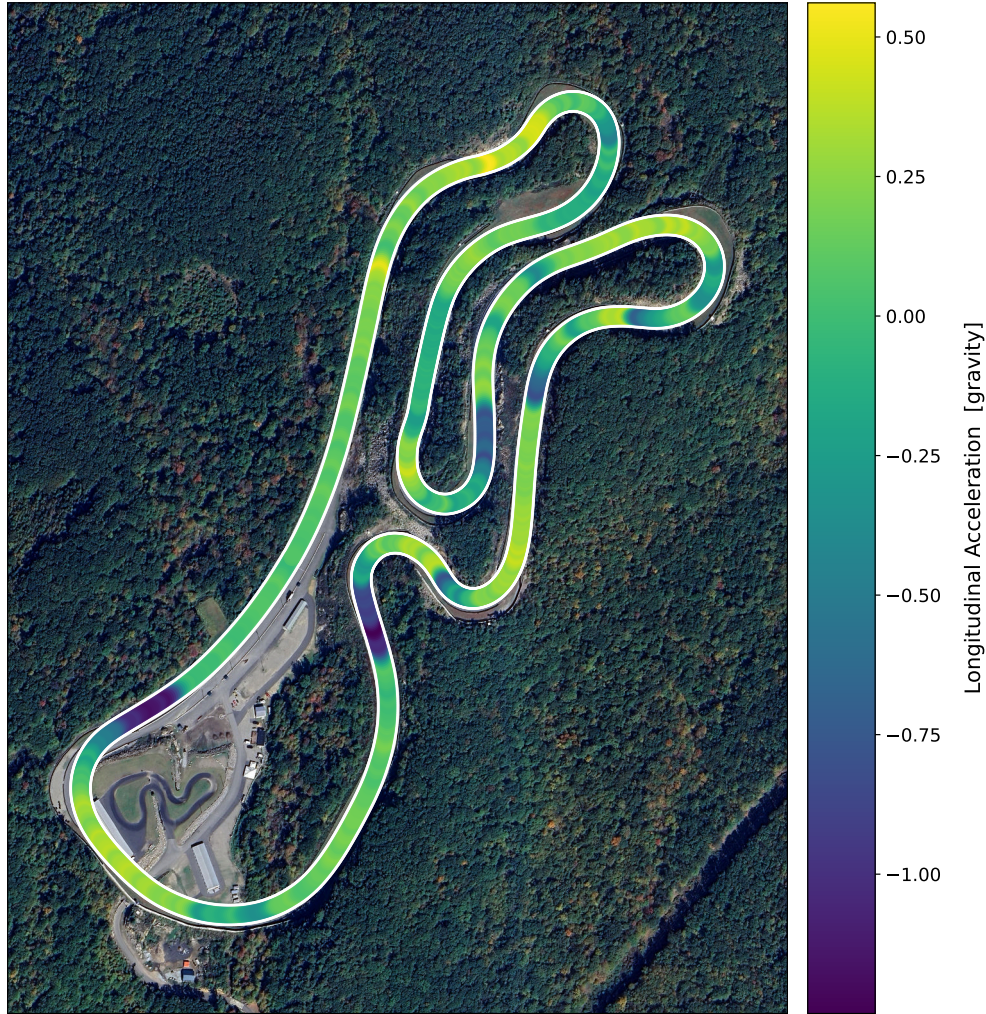
Figure 3.10: RUSH SR Longitudinal Acceleration for a Lap at Palmer Motorsports Park

the Podium Club Racetrack has been analyzed to provide insights into how these estimations vary throughout different track conditions and driving scenarios.

The longitudinal acceleration plot for Palmer Motorsports Park, illustrated in Figure 3.10, highlights the vehicle's acceleration and deceleration behavior over a complete lap at this racetrack. Acceleration values, expressed in units of gravity (g), provide insights into the vehicle's dynamic performance as it navigates the track.

Positive, yellower peaks in the plot indicate instances where the vehicle is accelerating forward, typically occurring right after a corner, in straight sections, or where the driver is applying the throttle to increase speed. Negative acceleration values represent deceleration or braking periods, where the overall kinetic energy of vehicle decreases and energy is (typically) dissipated as heat through the brakes.

These periods of negative acceleration can be capitalized to improve the overall efficiency of

the vehicle and reduce the size of the battery with a regenerative braking system in-place. Consistent and significant negative acceleration spikes suggest effective energy recapture by the regenerative braking system, especially important in a track environment where braking is frequent and energy recuperation opportunities are abundant.

Figure 3.11: RUSH SR Longitudinal Acceleration for a Lap at the Podium Club Racetrack

The longitudinal acceleration data for Podium Club, depicted in Figure 3.11, shows similar patterns of acceleration and deceleration as the vehicle completes a lap. Positive, yellower spikes again signify forward acceleration, likely occurring in straightaways or in less complex turns where maximum throttle can be applied. Negative spikes, indicating deceleration or braking, are of particular interest in assessing the regenerative braking system's performance.

In comparison to the Palmer track, variations in the Podium Club's track layout and driving demands are reflected in the acceleration profile. These differences provide valuable insights into how the regenerative braking system adapts to different racing environments. The depth and frequency of negative acceleration events on the Podium Club track will highlight the system's effectiveness in capturing energy across varied driving conditions.

Analyzing the data in Table 3.3, several interesting statistics emerge that highlight the performance and efficiency of the regenerative braking system under different track conditions. For instance, the mean longitudinal acceleration for both tracks is relatively low (0.01 g), suggesting an overall balanced performance between acceleration and deceleration. However, the standard deviation is higher at the Podium Club Racetrack (0.39 g) compared to Palmer Motorsports Park (0.32 g), indicating more variability in acceleration and braking events, which could imply more frequent or intense energy recuperation opportunities. This also

Table 3.3: RUSH SR Longitudinal Acceleration Statistics (in g) at Palmer Motorsports Park and the Podium Club Racetrack

Longitudinal Acceleration [g]	Palmer Motorsports Park	Podium Club Racetrack
Mean	0.01	0.01
Standard Deviation	0.32	0.39
Minimum	-1.25	-1.21
5th Percentile	-0.72	-0.91
10th Percentile	-0.41	-0.58
25th Percentile	-0.13	-0.19
Median (50th Percentile)	0.09	0.13
75th Percentile	0.22	0.27
90th Percentile	0.31	0.37
95th Percentile	0.36	0.4
Maximum	0.56	0.66

aligns with the observations drawn from the throttle usage data discussed in section 3.5.1.

The minimum values of longitudinal acceleration, -1.25 g at Palmer and -1.21 g at Podium, indicate significant deceleration events, which are critical for regenerative braking. The 5th percentile values (-0.72 g at Palmer and -0.91 g at Podium) further highlight these deceleration phases, suggesting that the regenerative braking system has ample opportunities to recapture energy.

By comparing the longitudinal acceleration data from both racetracks, conclusions can be drawn about the regenerative braking system's performance under different conditions. Effective regenerative braking is characterized by distinct and consistent patterns of negative acceleration during braking events. Such patterns suggest that the system reliably captures and converts kinetic energy into electrical energy. The consistency of these braking profiles across multiple laps indicates the reliability and efficiency of the system. Furthermore, the magnitude of negative acceleration provides additional insights into the amount of energy being recaptured. More profound negative acceleration values correlate with greater energy recuperation, which enhances the vehicle's overall efficiency, performance, and enables a smaller battery to be used.

In summary, analyzing longitudinal acceleration data from racetrack laps offers a detailed view of a hybrid vehicle's regenerative braking system's functionality. By examining acceleration and deceleration patterns on the Palmer Motorsports Park and Podium Club tracks, we gain a better understanding of how effectively the system operates in diverse driving scenarios. This analysis is crucial for optimizing the design and performance of regenerative braking systems in hybrid vehicles, contributing to advancements in automotive energy efficiency and sustainability.

3.7 Braking Analysis During Races

This section will discuss the different techniques and methods used to determine *when* the vehicle was braking.

3.7.1 Quantifying Braking

In section 3.6, periods of acceleration and deceleration, were determined mathematically, but this does not necessarily imply that the vehicle is undergoing *braking*. Therefore, a quantitative measure of braking is necessary to distinguish between mere deceleration and active braking, which is crucial for evaluating the effectiveness of the regenerative braking system.

To quantify braking, instances when the inline acceleration is less than -0.15 g were computed. This threshold is chosen based on empirical data and industry standards, indicating significant deceleration that typically corresponds to braking events. The output of this computation is binary: 0 when the brakes are not actively being applied, and 1 when the brakes are being applied.

This technique accurately identifies when the vehicle is actively braking. This binary output allows for a straightforward integration into data analysis processes, facilitating the assessment of the regenerative braking system's performance. The distinction between deceleration due to coasting or natural vehicle dynamics and actual braking is vital for understanding energy recovery efficiency and the overall effectiveness of the braking system. This quantification method provides a clear and objective measure to evaluate the regenerative braking system, ensuring that only relevant braking events are considered in the analysis.

Figure 3.12 highlights periods of active braking at Palmer Motorsports Park. These sections of the track will be used to estimate the cumulative amount of energy that can be recuperated through regenerative braking. The data indicates specific segments where the braking system is engaged, providing a detailed map of potential energy recovery zones. This detailed information can then be utilized to enhance the design and efficiency of regenerative braking systems by focusing on high-frequency braking areas.

Similarly, Figure 3.13 highlights periods of active braking at the Podium Club Racetrack. Sections of the track where braking occurs will be used to estimate the cumulative amount of energy that can be recuperated through regenerative braking. The comparison between different tracks, as shown in these figures, allows for a comprehensive understanding of how track design influences braking patterns and the potential for energy recovery.

Compared to Palmer's braking profile as depicted in Figure 3.12, the Podium track, depicted in Figure 3.13, has far more consistent and frequent periods of braking. This observation suggests that the Podium track offers greater opportunities for energy recuperation due to
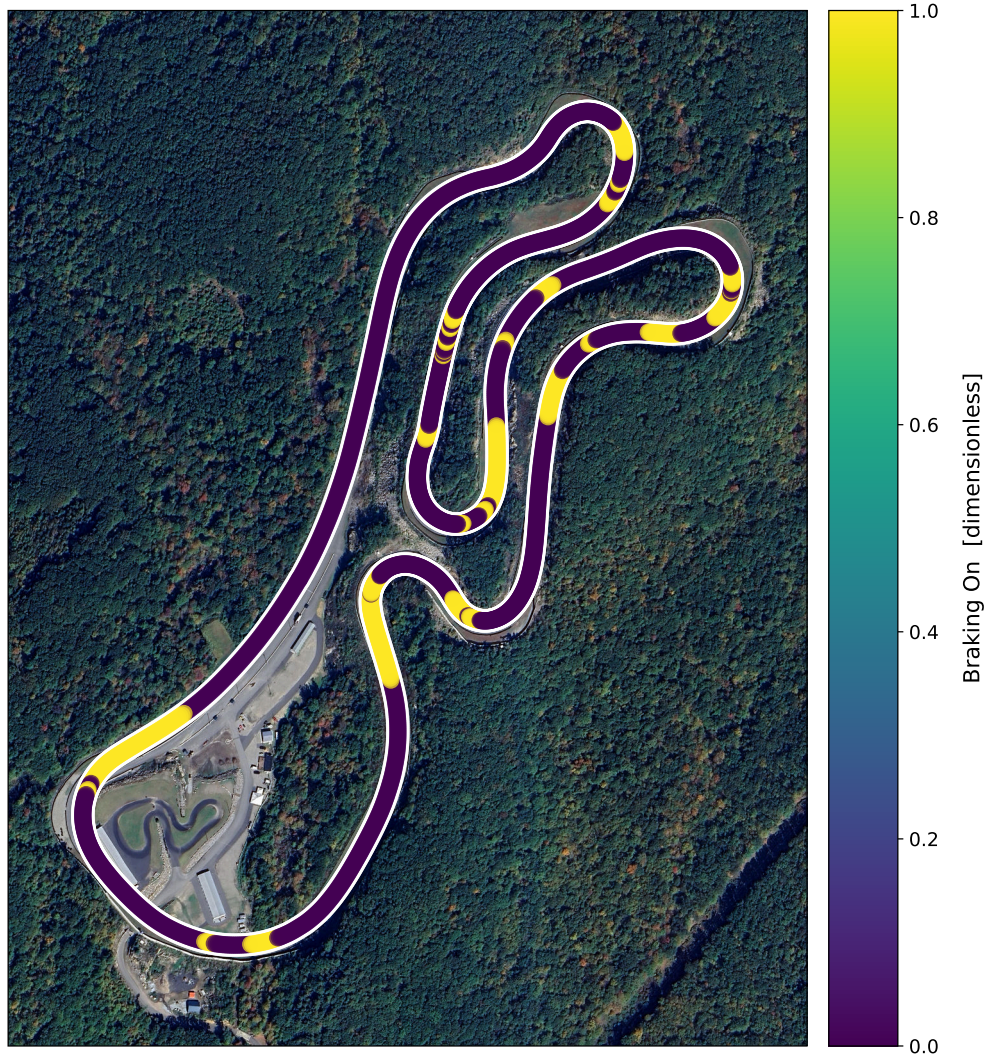
Figure 3.12: RUSH SR Braking On for a Lap at Palmer Motorsports Park

more frequent braking events. The variability in braking patterns across different tracks emphasizes the importance of tailored regenerative braking strategies for each specific track to maximize energy recovery.

3.7.2 Braking Pressure

The analysis of the Palmer racetrack braking data, as illustrated in Figure 3.14, reveals that the braking pressure fluctuates between 0.5 to 2.5 volts. When the brakes are not in use, they generally idle at 0.5 volts. This variation in braking pressure is indicative of the driver's response to the racetrack's layout, which includes a series of turns and straightaways requiring different levels of braking intensity.
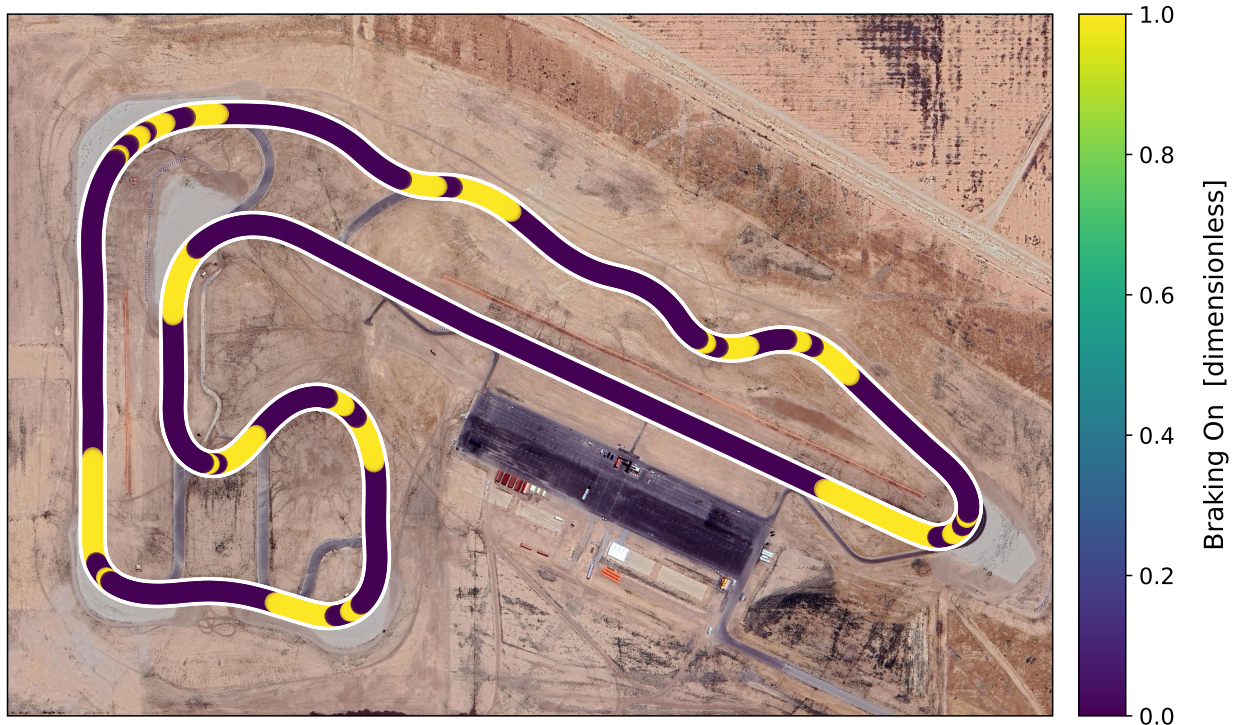
Figure 3.13: RUSH SR Braking On for a Lap at the Podium Club Racetrack

Peaks in the braking pressure graph correspond to segments of the track where significant braking force is necessary, likely due to sharp turns or approaching corners. The relatively lower range of braking pressures observed at the Palmer racetrack suggests a less demanding braking scenario, where the regenerative braking system can operate efficiently without reaching its maximum capacity. This suggests that the battery might not be recharged as frequently as other racing scenarios.

In contrast, the Podium racetrack data, highlighted in Figure 3.15, presents a different narrative, with braking pressure ranging from 0.5 to 4.5 volts. The increased range and higher peaks in braking pressure indicate that the Podium track imposes more rigorous braking demands on the vehicle. This can be attributed to the track's design, which may include tighter corners, more frequent braking zones, and possibly elevation changes that necessitate greater braking force. By capturing more energy during high-pressure braking events, a regenerative braking system could significantly contribute to the vehicle's overall efficiency.

3.7.3 Comparing Braking Pressure Across Race Tracks

A comparative analysis of the braking pressure data from the Palmer and Podium racetracks underscores the potential regenerative braking system's versatility and effectiveness. Braking and Throttle Percentages are overlaid in Figure 3.16. The Podium track, with its broader
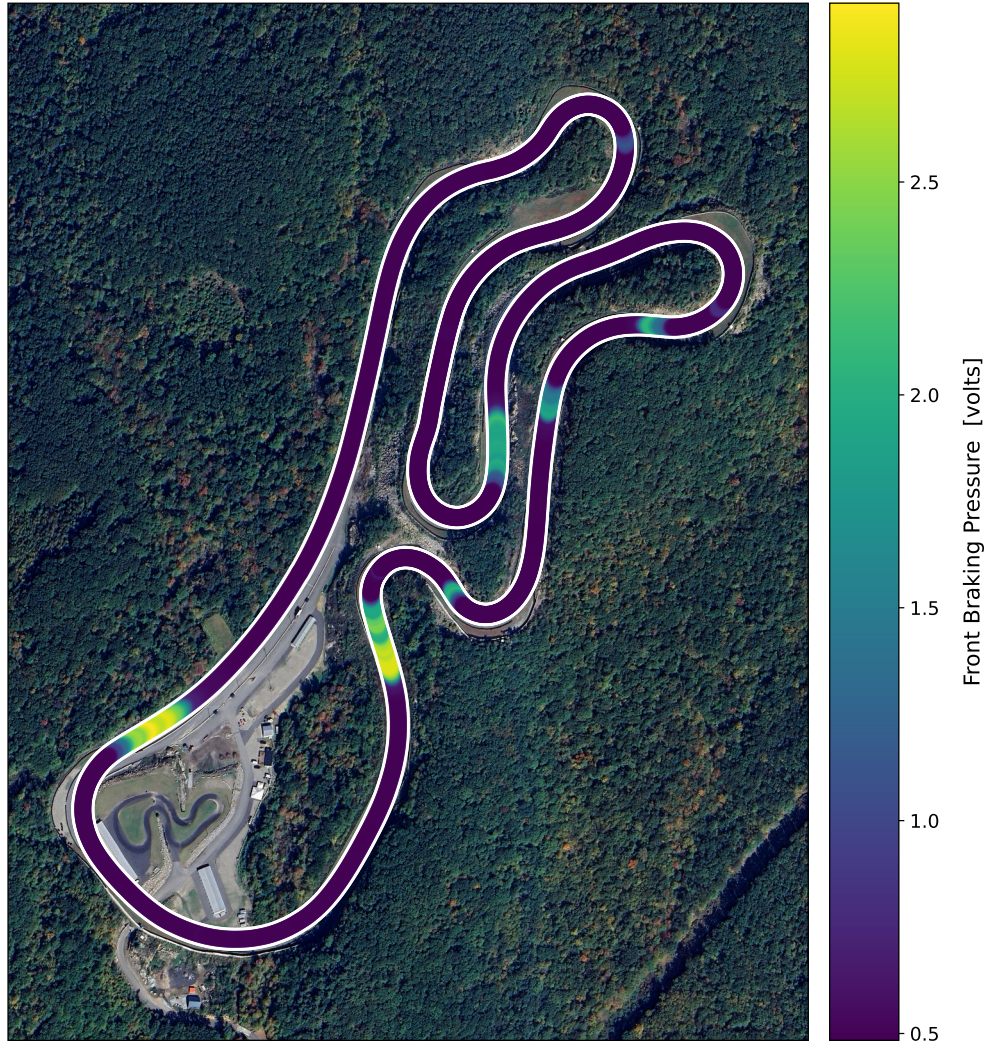
Figure 3.14: RUSH SR Braking Pressure for a Lap at Palmer Motorsports Park

range of braking pressures and higher peak values, exemplifies a more ideal environment for the braking system, as there are more frequent periods of braking allowing the battery to be "topped off" throughout the race relatively consistently. This track demands greater braking forces, which the regenerative system manages adeptly, thereby maximizing energy recovery.

On the other hand, the Palmer track, with its lower and less frequent braking pressures, represents a less intensive scenario where the battery would be recharged less frequently, but with greater magnitudes. This comparison illustrates the system's ability to adapt to different racing conditions, ensuring optimal performance across diverse environments. Such adaptability is crucial for hybrid vehicles, as it enhances their energy efficiency and overall performance by leveraging regenerative braking technology to its fullest potential.

The analysis of front braking pressure on the Palmer and Podium racetracks provides valuable insights into the performance and effectiveness of the regenerative braking system in a
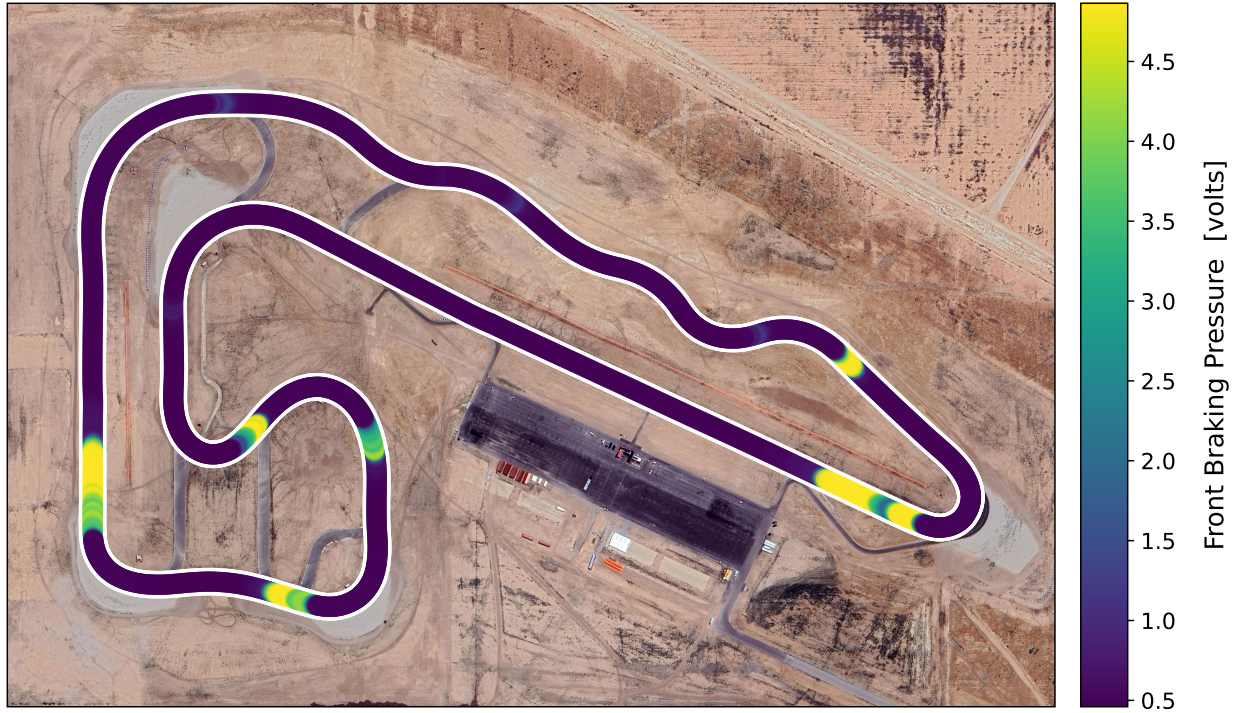
Figure 3.15: RUSH SR Braking Pressure for a Lap at the Podium Club Racetrack

(a) Palmer Motorsports Park

(b) Podium Club Racetrack
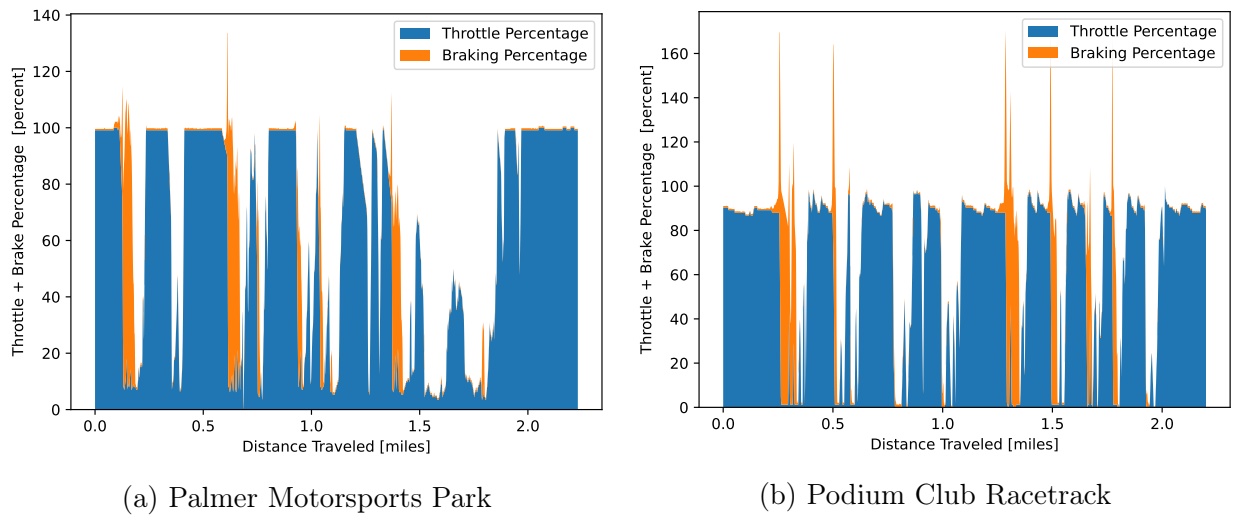
Figure 3.16: RUSH SR Throttle and Brake Usage: (a) Throttle and Brake Usage of a Lap at Palmer Motorsports Park; (b) Throttle and Brake Usage of a Lap at the Podium Club Racetrack.

hybrid vehicle. The Palmer racetrack data highlights the need for the regenerative braking system to maintain consistent performance despite relatively infrequent recharging periods. The Podium racetrack data, on the other hand, showcases its robustness under more intensive, consistent conditions where it has frequent opportunities to recharge its batteries.

These findings are instrumental in optimizing the regenerative braking system for diverse racing environments, contributing to the advancement of hybrid vehicle technology and its application in motorsports.

Chapter 4

Energy Recuperation Estimates During Braking

This chapter analyzes the estimation of energy recuperation during braking to using the race data analyses described in chapter 3. Section 4.1 revisiting Newton's Laws of Motion and the fundamental principles that govern vehicle behavior during acceleration and braking, providing a foundational understanding necessary for subsequent analyses. The relationship between acceleration and energy is discussed in section 4.2, highlighting how kinetic energy is transformed during braking and how regenerative braking systems can capture a portion of this energy to enhance efficiency and charge a battery. Empirical data on regenerative braking efficiency, including estimates from laps at Palmer Motorsports Park and the Podium Club Racetrack, are presented in section 4.3 to get an accurate estimate of real-world energy recuperation potential. Both instantaneous and cumulative energy recovery insights are reviewed. By integrating theoretical principles with practical data, this chapter provides a comprehensive examination of how regenerative braking can significantly contribute to the overall energy efficiency of hybrid vehicles.

4.1 Newton's Laws of Motion in the Context of Vehicle Dynamics and Energy Recuperation

To further understand the dynamics of the vehicle's acceleration and the effectiveness of its regenerative braking system, it is essential to revisit Isaac Newton's Laws of Motion and their application to vehicular motion and energy transformations. Newton's laws provide the fundamental principles that govern the behavior of objects in motion, which are directly relevant to the analysis of acceleration and braking in this context.

4.1.1 Law of Inertia

Newton's First Law, often referred to as the Law of Inertia, states that an object remains at rest or in uniform motion in a straight line unless acted upon by an external force [24]. In the context of vehicle dynamics, this law explains why a car continues to move at a constant speed unless external forces like friction, air resistance, or braking forces act upon it.

4.1.2 Law of Acceleration

Newton's Second Law, the Law of Acceleration, states that the acceleration of an object is directly proportional to the net force acting on it and inversely proportional to its mass. This is mathematically expressed as equation (4.1):

$$F = ma \tag{4.1}$$

where F is the net force, m is the mass, and a is the acceleration.

For a vehicle, this law illustrates how changes in the net force, such as those caused by engine thrust or braking, result in changes in acceleration.

4.1.3 Action-Reaction Law

Newton's Third Law, the Action-Reaction Law, states that for every action, there is an equal and opposite reaction. This principle is crucial in understanding braking systems, including regenerative braking, where the braking force exerted by the system on the wheels has a reaction force that decelerates the vehicle. In conventional vehicle braking systems, this reaction force involves using brake pads and friction to mechanically reduce the velocity of the vehicle.

4.2 Relating Acceleration to Energy

Acceleration, as derived from Newton's Second Law, is a critical factor in understanding the energy transformations in a vehicle. When analyzing a vehicle's longitudinal acceleration, we can relate it to the kinetic energy and the work done by the braking system, particularly the regenerative braking system. The kinetic energy of a vehicle is given by equation (4.2):

$$KE = \frac{1}{2}mv^2 \tag{4.2}$$

where m is the mass of the object in motion (in this case, the vehicle and driver) and v is its velocity.

During acceleration, the engine does work to increase the vehicle's kinetic energy, while during deceleration, such as in braking, the vehicle's kinetic energy decreases.

In regenerative braking systems, the kinetic energy lost during deceleration is not merely dissipated as heat, as in conventional braking, but is converted into electrical energy to recharge the vehicle's batteries. The amount of energy recuperated can be estimated by analyzing the deceleration (negative acceleration) phases. The work done by the braking system (regenerative work W) to decelerate the vehicle can be represented as equation (4.3):

$$W = \Delta KE = \frac{1}{2}m(v_f^2 - v_i^2) \tag{4.3}$$

where v_f is the final velocity after a given time period and v_i is the initial velocity. This equation shows the change in kinetic energy, which corresponds to the amount of energy that can potentially be recaptured by the regenerative braking system.

During a deceleration event captured in the longitudinal acceleration plot, the negative acceleration a can be linked to the reduction in kinetic energy. The force applied by the braking system F_{Brake} is given by $F_{Brake} = ma$. The power $P_{Braking}$ converted by the regenerative braking system can be approximated by the product of this force and the vehicle's velocity v, expressed as equation (4.4):

$$P_{Braking} = F_{Brake}v = mav \tag{4.4}$$

This power represents the rate at which kinetic energy is being dissipated during braking. Integrating this power over the deceleration time period gives the total energy recaptured, modeled in equation (4.5).

$$E_{Braking}^{Total} = \int_{Braking} P \cdot dt \tag{4.5}$$

By applying Newton's Laws of Motion and the principles of energy conservation, we can quantitatively analyze the effectiveness of the regenerative braking system. Understanding these relationships allows for deeper insights into how well the system converts kinetic energy into electrical energy and how this impacts the vehicle's overall performance and efficiency. This mathematical framework underscores the importance of detailed longitudinal acceleration data in evaluating and optimizing regenerative braking systems in hybrid vehicles.

4.3 Regenerative Braking Estimates

4.3.1 Regenerative Braking Assumptions and Baseline Parameters

Based on prior analyses of the capabilities of electric vehicles and electric motors, consensus has been reached that a conservative efficiency value for regenerative braking is approximately $\eta_{Regen} = 25\%$ [25]–[28]. This means that approximately 25% of the energy dissipated during braking could actually be recovered using a well-designed regenerative braking system. Therefore, the energy recovery estimates can be modeled using equation (4.6).

$$
\begin{aligned}
E_{Braking}^{Regen} &= \eta_{Regen} \times \int_{Braking} P \cdot dt \\
E_{Braking}^{Regen} &= 25\% \times \int_{Braking} mav \cdot dt
\end{aligned}
\tag{4.6}
$$

To evaluate the overall effectiveness of a regenerative braking system for all different laps, the total energy recovered during a lap is normalized by the length of the race track. This is described using equation (4.7), where l_{Track} is the length of the race track.

$$
\text{Regen per Mile} = \frac{E_{Braking}^{Regen}}{l_{Track}}
\tag{4.7}
$$

4.3.2 Cumulative Regenerative Braking Energy Recuperation Estimates for a Single Lap

To accurately estimate the amount of energy that could be recovered through regenerative braking, equation (4.6) was used, as described in section 4.3.1. The plots provided in Figure 4.1 and Figure 4.2 analyze vehicle energy recovery through regenerative braking systems on two racetracks: Palmer Motorsports Park and the Podium Club Racetrack. The periods where no energy recovery occurs are shaded in gray, allowing for a clear distinction between active energy recovery phases and inactive ones.

4.3.2.1 Palmer Motorsports Park Energy Recovery Visualization

In Figure 4.1, the kinetic energy recuperated during braking is displayed over the course of a lap. The data shows multiple peaks (yellow zones) where energy is recuperated, with several gray-shaded areas indicating periods with no energy recovery (as the vehicle is accelerating or
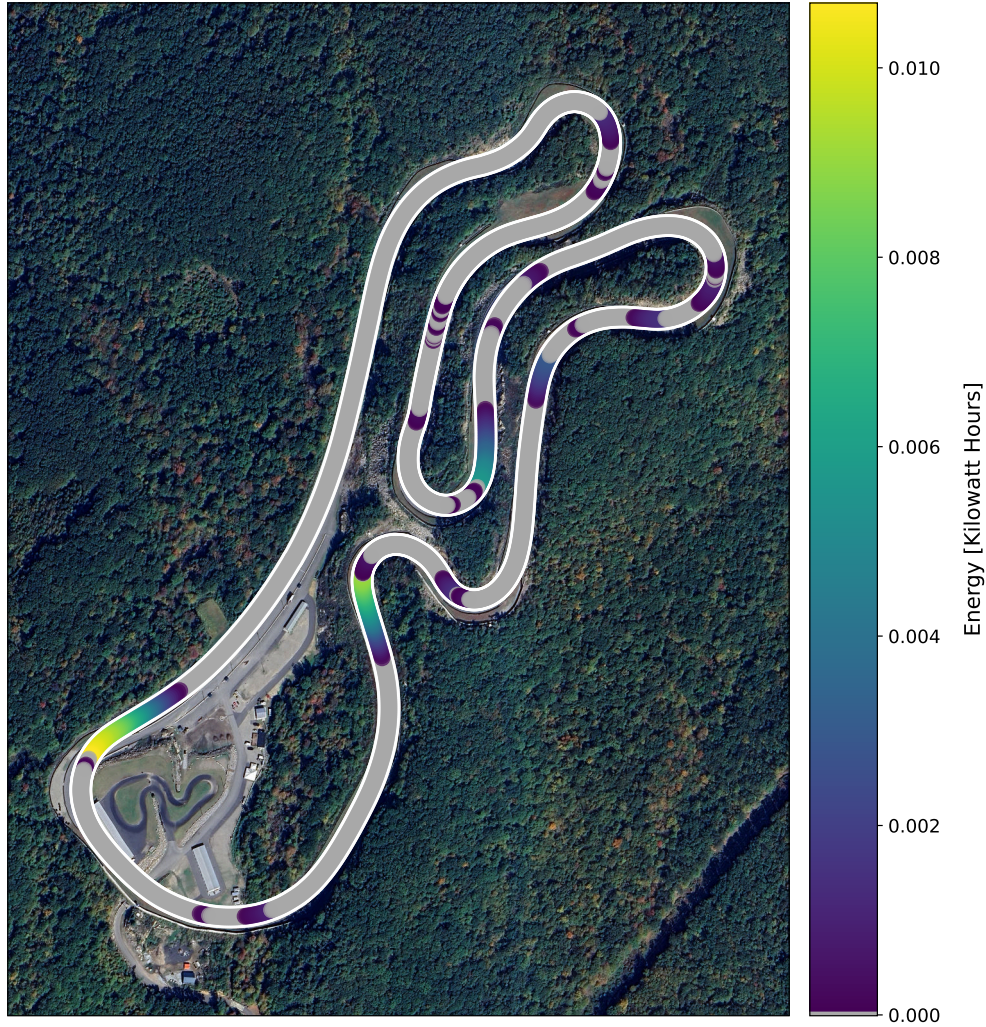
Figure 4.1: Map of the Regenerative Braking Energy Recovery Estimates for a Single Lap at Palmer Motorsports Park

coasting during those periods). Energy recuperation corresponds with braking zones where the driver is actively decelerating the vehicle, and a portion of the energy typically dissipated as heat is recovered and stored as electrical energy in the battery.

4.3.2.2 Podium Club Racetrack Energy Recovery Visualization

At the Podium Club Racetrack, as detailed in Figure 4.2, kinetic energy recovery spikes at various points, with a maximum around 0.012 kWh per lap. Despite the fact that the two racetracks are approximately the same length, as discussed in section 3.4, the nature of the Podium racetrack lends itself to more periods of high velocities, leading to higher magnitude deceleration events.

Figure 4.2: Map of the Regenerative Braking Energy Recovery Estimates for a Single Lap at the Podium Club Racetrack

4.3.3 Cumulative Energy Recovery During a Single Lap

(a) Palmer Motorsports Park

(b) Podium Club Racetrack
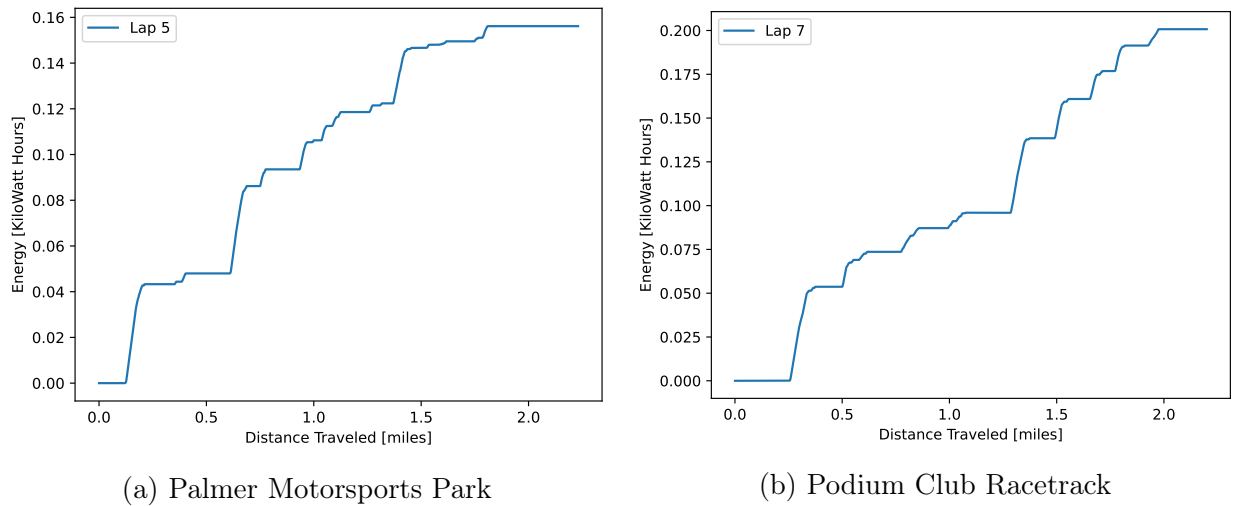
Figure 4.3: RUSH SR Regenerative Braking Energy Recuperation Estimates for a Single Lap: (a) Palmer Motorsports Park; (b) Podium Club Racetrack.

Figure 4.3 shows the regenerative braking energy recuperation estimates for a single lap at Palmer Motorsports Park (Figure 4.3a) and the Podium Club Racetrack (Figure 4.3b), respectively. Both graphs plot the energy recovered (in kWh) against the distance traveled

(in miles). Over the course of the race, typically before tight corners, the driver decelerates the vehicle which allows for periods of energy recovery.
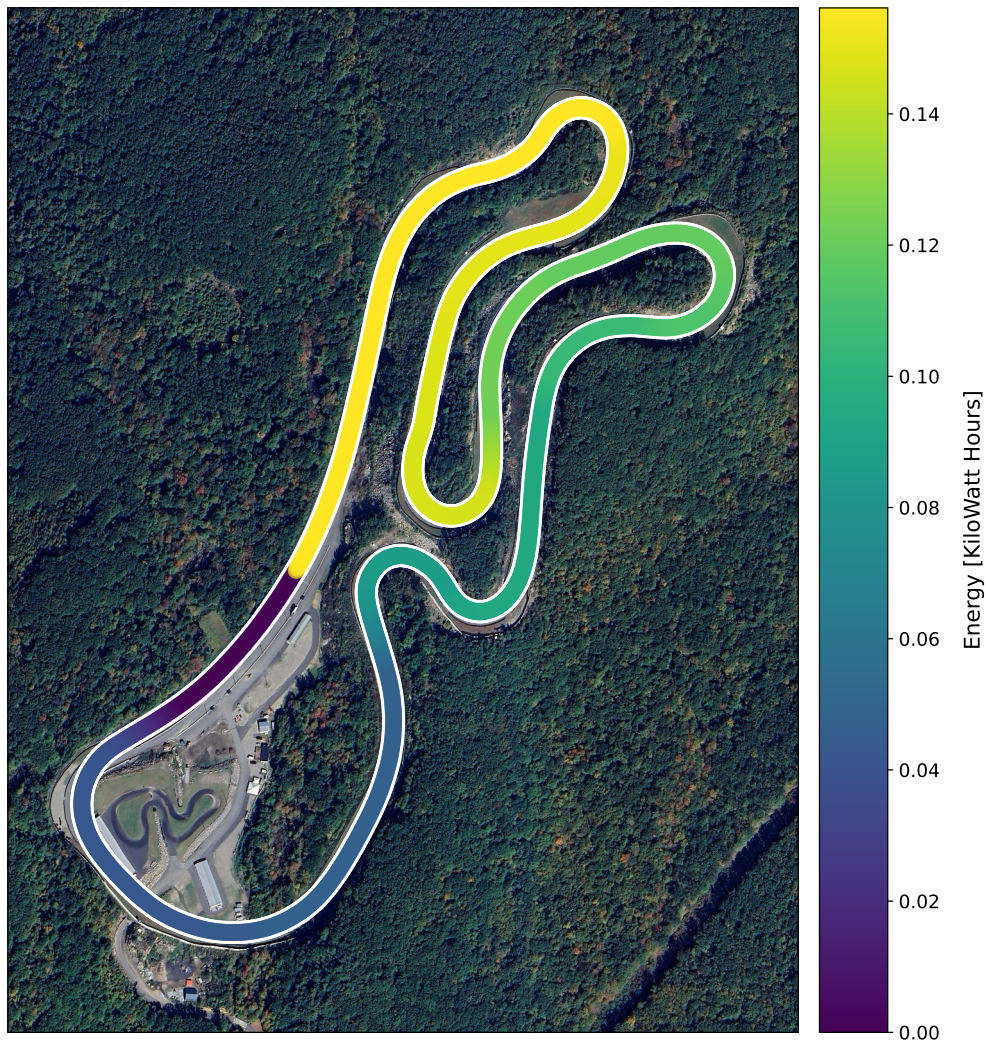
Figure 4.4: Map of the Estimated Cumulative Energy Recovered from Regenerative Braking for a Single Lap at Palmer Motorsports Park

At Palmer Motorsports Park, the energy recovery starts close to the beginning of the lap and shows a gradual increase with a notable rise around the mid-point of the lap, as detailed in Figure 4.3a. This aligns with the locations of straightaways and tight corners, as shown in Figure 4.4. After a long straightaway, the vehicle is traveling near its top speed (as discussed in greater detail in section 3.4), and then quickly decelerates to prepare for a sharp turn (as discussed in greater detail in section 3.6). Overall, the total energy recovered in a single lap reaches approximately 0.16 kWh.

Similarly, at the Podium Club Racetrack, the energy recovery also begins promptly and exhibits a steady increment throughout the lap, as detailed in Figure 4.3b. Due to the nature of the Podium Club Racetrack's design, regenerative braking occurs more consistently
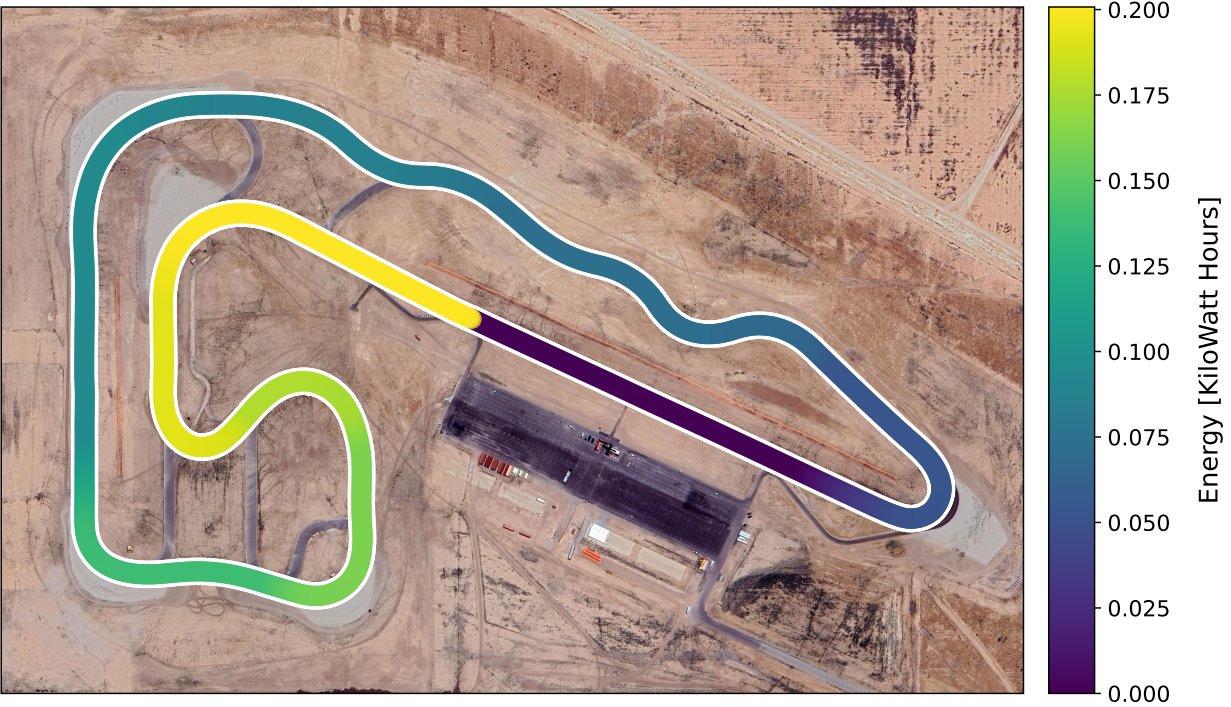
Figure 4.5: Map of the Estimated Cumulative Energy Recovered from Regenerative Braking for a Single Lap at the Podium Club Racetrack

throughout the lap, depicted by the more gradual color-shift observed in Figure 4.5. Ultimately, it is estimated that approximately 0.20 kWh of energy could be recovered over the course of a single lap at the Podium Club.

These plots indicate that significant energy recovery could occur during a single lap of a race, suggesting that the integration of a regenerative braking system can provide substantial energy savings. For a hybrid vehicle, this recovered energy can be redirected to the battery, potentially reducing the size of the battery pack required for the race, resulting in lowered costs, reduced weight, and increased performance.

4.3.4 Cumulative Energy Recovery Estimates Through Regenerative Braking for Multiple Laps

Figure 4.6 extends the analysis presented in section 4.3.2 to multiple laps, comparing cumulative energy recovery for each lap of both races.
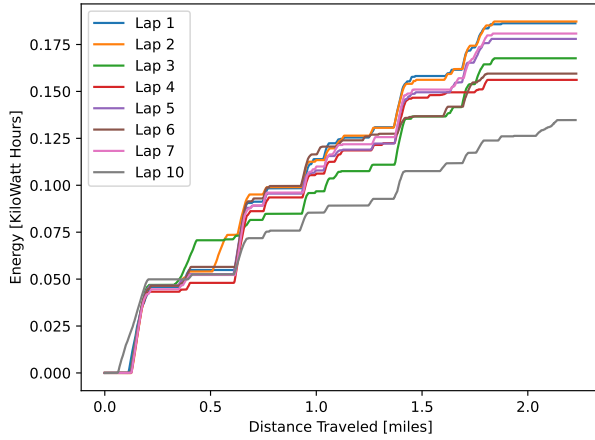
(a) Palmer Motorsports Park
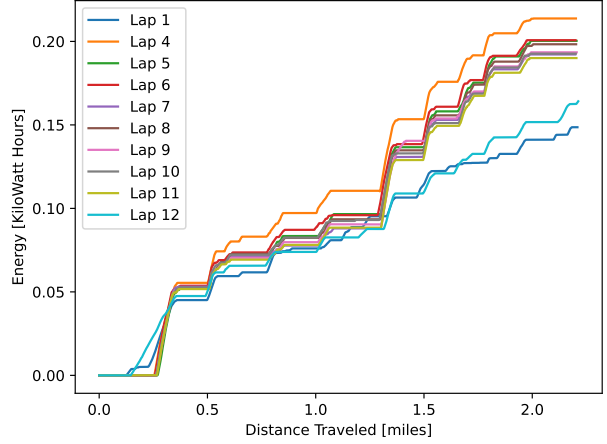
(b) Podium Club Racetrack

Figure 4.6: RUSH SR Regenerative Braking Energy Recuperation Estimates for All Laps: (a) All Laps at Palmer Motorsports Park; (b) All Laps at the Podium Club Racetrack.

4.3.4.1 Regenerative Braking Estimates for a Race at Palmer Motorsports Park

At Palmer Motorsports Park, the cumulative energy recovery is quite consistent across all laps, indicating that energy recuperation capabilities do not deviate tremendously lap-to-lap when the vehicle is driven aggressively for a race, as show in Figure 4.6a. The 'linear-ish' nature of the energy recovery graphs suggest that the frequency and magnitude of braking periods along the track are relatively evenly-distributed.

Table 4.1: Estimated Energy Recovery Through Regenerative Braking for a Race at Palmer Motorsports Park

Lap	Lap Time	Total Energy Recovered [Wh]	Smallest Period of Regen [Wh]	Time [s]	Largest Period of Regen [Wh]	Time [s]
Lap 1	1:45.659	186.31	0.0752	0.30	11.45	4.55
Lap 2	1:41.236	187.25	0.1645	0.40	11.62	3.55
Lap 3	1:43.876	167.65	0.0973	0.30	11.72	3.85
Lap 4	1:54.879	156.15	0.0138	0.15	10.68	3.35
Lap 5	1:46.356	177.98	0.0271	0.15	11.65	4.05
Lap 6	1:40.942	159.49	0.0236	0.15	11.14	3.40
Lap 7	1:54.410	180.83	0.0246	0.25	10.48	3.05
Lap 10	1:40.493	134.74	0.0065	0.20	12.47	6.10
Average	1:45.981	168.80	0.0541	0.24	11.40	3.99

Looking at each lap's individual metrics, detailed in Table 4.1, it is found that most laps

closely resemble each other, with the cumulative energy for slower laps not necessarily resulting in lower overall energy recovery. The average lap time was 1:45.981, and the average energy recovered during these laps was 0.1688 kWh. Laps 4 and 7 were notably slower than the others, but the total energy recovered during these laps, with times of 1:54.879 and 1:54.410 respectively, was 0.15615 kWh and 0.18083 kWh respectively.

Lap 10 stands out with the lowest energy recovery of 0.13474 kWh, which could be attributed to less overall braking or more coasting. The smallest periods of regeneration show minor variations, with an average of 0.0541 Wh. However, the largest periods of regeneration show more significant differences, ranging from 10.48 Wh to 12.47 Wh, indicating variable braking intensity or opportunities for energy capture.

$$\text{Regen per Mile at Palmer} = \frac{E_{Braking}^{Regen}}{l_{Track}} = \frac{0.1688 \text{ kWh}}{2.3 \text{ Miles}} = 0.07339 \frac{\text{kWh}}{\text{Mile}} \tag{4.8}$$

Normalizing the average energy recovered through regenerative braking by the length of the Palmer race track, it is found that the driver was able to recover approximately $0.07339 \frac{\text{kWh}}{\text{Mile}}$ (4.8).

4.3.4.2 Regenerative Braking Estimates for a Race at the Podium Club Racetrack

Like Palmer, the Podium Club Racetrack also demonstrates similar consistent trends for regenerative braking.

While the average energy recovered at Palmer Motorsports Club was 0.16880 kWh over the 2.3 mile track, the Podium Club Racetrack recovered an average of 0.18943 kWh per lap, even though the lap was 2.32 miles in length.

Looking at each lap's individual metrics, detailed in Table 4.2, it is found that most laps closely resemble each other, with the cumulative energy for slower laps not necessarily resulting in lower overall energy recovery. The average lap time was 1:39.493, and the average energy recovered during these laps was 0.18943 kWh. Laps 1 was notably slower than the others, taking 1:47.355, and the total energy recovered during this lap was 0.14861 kWh.

Lap 1 and Lap 12 stand out with the lowest energy recovery of 0.14861 kWh and 0.16415 kWh respectively, which could be attributed to less overall braking or more coasting. The smallest periods of regeneration show minor variations, with an average of 0.0762 Wh being recovered when the driver taps the brakes. The largest periods of regeneration show more significant differences, ranging from 9.85 Wh to 13.16 Wh, indicating variable braking intensity or opportunities for energy capture.

Table 4.2: Estimated Energy Recovery Through Regenerative Braking for a Race at the Podium Club Racetrack

Lap	Lap Time	Total Energy Recovered [Wh]	Smallest Period of Regen [Wh]	Time [s]	Largest Period of Regen [Wh]	Time [s]
Lap 1	1:47.355	148.61	0.0155	0.15	9.85	6.40
Lap 4	1:41.761	213.75	0.0374	0.15	13.85	5.30
Lap 5	1:39.183	200.34	0.2639	0.60	12.36	3.85
Lap 6	1:37.072	200.74	0.0927	0.25	12.85	4.15
Lap 7	1:38.608	192.19	0.0508	0.25	13.16	4.45
Lap 8	1:37.040	198.30	0.2638	0.45	12.56	3.85
Lap 9	1:37.154	193.47	0.0083	0.10	12.70	4.10
Lap 10	1:41.524	192.67	0.0143	0.15	12.97	4.95
Lap 11	1:37.626	190.04	0.0132	0.20	12.40	3.80
Lap 12	1:37.612	164.15	0.0101	0.15	11.88	9.80
Average	1:39.493	189.43	0.0762	0.25	12.46	5.07

$$\text{Regen per Mile at Podium} = \frac{E_{Braking}^{Regen}}{l_{Track}} = \frac{0.18943 \text{ kWh}}{2.32 \text{ Miles}} = 0.08165 \frac{\text{kWh}}{\text{Mile}} \qquad (4.9)$$

Normalizing the average energy recovered through regenerative braking by the length of the Podium race track, it is found that the driver was able to recover approximately 0.08165 $\frac{\text{kWh}}{\text{Mile}}$ (4.9). This is very similar to the normalized energy recovery estimated for Palmer, which was 0.07339 kWh.

Chapter 5

Battery Specifications and Sizing

This chapter explores the crucial aspects of battery specifications and sizing, providing a comprehensive analysis necessary for understanding the selection and implementation of battery technologies in various applications. The chapter is structured to cover a broad range of topics starting with a historical overview of battery technologies in Section 5.1, tracing the evolution from Volta's voltaic pile to modern lithium-ion batteries. This historical context sets the stage for a detailed comparison of different battery technologies in Section 5.2, where subsections delve into the specifics of lead-acid and lithium-ion batteries, discussing their energy densities, benefits, and drawbacks. The chapter then transitions to practical applications, focusing on the process of sizing battery packs without regenerative braking in Section 5.3, followed by an analysis of battery sizing with regenerative braking in Section 5.4. Each section not only examines the theoretical underpinnings and innovations in battery technology but also provides practical equations and data tables to aid in understanding the trade-offs and considerations involved in selecting and sizing batteries for specific uses. This comprehensive approach ensures that readers gain a thorough understanding of both the historical development and contemporary applications of battery technologies.

5.1 A Brief History of Batteries and Battery Technologies

Battery technologies have evolved significantly since Alessandro Volta's invention of the voltaic pile in 1800, the first electrochemical cell that could provide a steady current [29]. This invention laid the groundwork for the development of modern batteries, sparking the progression from basic chemical energy storage to sophisticated and high-efficiency battery systems used today in a variety of different applications.

Volta's contribution marked the beginning of electrochemistry, demonstrating that electricity could be generated chemically. His voltaic pile, composed of alternating discs of zinc and

copper separated by brine-soaked cardboard, provided a continuous flow of electricity and showcased the practical potential of chemical energy storage. This innovation catalyzed further developments in battery technology over the centuries.

Following Volta's breakthrough, the 19th century saw the advent of the lead-acid battery in 1859 by Gaston Planté, which became the first rechargeable battery and is still widely used in various applications due to its reliability and low cost [30]. However, lead-acid batteries suffer from low energy density and significant weight, limiting their use in high-demand applications.

The progression of battery technology saw the development of nickel-cadmium batteries in 1899, offering improved storage capacity but plagued by the memory effect, affecting their voltage stability over time [31]. Subsequent advancements led to the creation of nickel-metal hydride and ZEBRA batteries before the commercial introduction of lithium-ion batteries in 1991 by Sony [32]. Lithium-ion batteries quickly became predominant due to their high specific energy, long cycle life, and efficiency, despite drawbacks such as high costs and the need for sophisticated safety and monitoring systems [33].

Lithium-ion batteries encompass several chemistries, each with unique properties and applications. These include Lithium Cobalt Oxide ($LiCoO_2$), Lithium Nickel Manganese Cobalt Oxide (NMC), Lithium Iron Phosphate ($LiFePO_4$), and Lithium Nickel Cobalt Aluminum Oxide (NCA) [31]. $LiCoO_2$ batteries, known for their high energy density, are widely used in consumer electronics but have limited thermal stability and higher costs due to cobalt. NMC batteries, combining nickel and manganese, are favored for their balance of specific energy, thermal stability, and cost, making them suitable for EVs like the Nissan Leaf and BMW i3 [34]. $LiFePO_4$ batteries offer excellent thermal stability and safety, making them ideal for applications requiring high power and safety, such as electric buses. NCA batteries, used by Tesla, offer high specific energy and power but at higher costs and with safety concerns [35].

Beyond traditional Lithium-ion batteries, emerging technologies such as Lithium-Sulfur (Li-S) and Lithium-Air ($Li-O_2$) batteries promise higher specific energies but face challenges like short cycle life and stability issues. Li-S batteries, for instance, can potentially offer five times the charging capacity of conventional Li-ion batteries but are not yet commercially viable due to issues like polysulfide dissolution during cycles [36].

5.2 Comparing Battery Technologies

5.2.1 Lead-Acid Batteries

Lead-acid batteries are characterized by their relatively low energy density compared to other battery types. Specifically, lead-acid batteries have a specific energy range of 30-40 $\frac{Wh}{kg}$ and an energy density of 60-75 $\frac{Wh}{L}$. This is significantly lower than lithium-ion batteries, which

can achieve specific energies up to 200 $\frac{\text{Wh}}{\text{kg}}$ and energy densities around 300 $\frac{\text{Wh}}{\text{L}}$. The high atomic weight of lead (Pb) is a primary factor limiting the specific energy and power density of lead-acid batteries [37].

Interestingly, lead-acid batteries are influenced significantly by relativistic effects, particularly due to the heavy atomic mass of lead. The energy differences arising from relativistic effects are substantial in heavy elements, as explained by Einstein's Theory of Relativity [38]. These effects primarily stabilize the 6s electrons in lead, thus increasing the oxidative power of lead dioxide (PbO_2) and contributing significantly to the overall cell voltage of the battery. Without these relativistic effects, the efficiency and functionality of lead-acid batteries would be much lower [39].

5.2.1.1 Innovations in Lead-Acid Battery Technology

Despite their lower energy density, lead-acid batteries have seen considerable innovations aimed at improving their performance and applicability. The shift from prismatic to spiral-wound cell geometry has led to significant enhancements to the power output and specific energy characteristics of lead-acid batteries.

Additionally, research has focused on improving the utilization of active materials (lead and lead dioxide) and reducing the share of non-active components, leading to nearly a two-fold increase in energetic characteristics over the past decades. Advanced additives such as Ti_4O_7 and SnO_2-coated flakes have been introduced to improve the conductivity and utilization of the positive active mass (PAM), further enhancing battery performance.

5.2.1.2 Benefits of Lead-Acid Batteries

The main benefits of Lead-Acid batteries include their cost, reliability, ability to deliver high power outputs, and their recyclability. They are one of the most economical rechargeable battery technologies in terms of cost per watt-hour, making them highly attractive for applications where budget constraints are significant. Having been in use for over a century, they've shown their reliability and robustness in a variety of applications, from automotive to stationary power sources. Capable of delivering high surge currents, they are ideal for applications requiring a short but high power event, such as automotive starter batteries. Lastly, approximately 95% of the materials used in lead-acid batteries are recyclable, which significantly reduces their environmental impact compared to other battery types.

5.2.1.3 Drawbacks of Lead-Acid Batteries

Despite the benefits discussed in Section 5.2.1.2, there are many major reasons why lead-acid batteries are not used in cellphones, electric vehicles, and other common battery use-cases.

Their low energy density, shorter lifespan, and environmental concerns make them the unideal choice for many applications.

Lead-acid batteries have a lower energy density compared to modern alternatives like lithium-ion batteries. This limits their use in applications where weight and space are critical factors, such as cellphones, laptops, and vehicles. They also tend to have a shorter cycle life compared to newer technologies, such as nickel-metal hydride and lithium-ion batteries. This means they may need to be replaced more frequently, especially in high-demand applications.

In summary, while lead-acid batteries offer several advantages in terms of cost, reliability, and recyclability, their lower energy density, shorter lifespan, and environmental concerns limit their applicability in certain high-performance and sensitive environments. Ongoing innovations aim to address these limitations and enhance the overall performance and safety of lead-acid battery technology.

5.2.2 Lithium-Ion Batteries

Lithium-Ion Batteries (LIBs) have revolutionized the landscape of energy storage technologies since their commercialization by Sony Corporation in 1991. Known for their high energy density, LIBs have become integral in powering a myriad of portable electronics, electric vehicles, and renewable energy storage systems. This section looks into the critical aspects of LIBs, including their energy density, key innovations, and the advantages and disadvantages of this technology [40].

5.2.2.1 Energy Density

Battery Type	Abbreviation	Energy Mass Density $\left[\frac{Wh}{kg}\right]$	Voltage [V]	Cycles
$LiFePO_4$	LFP	90-120	2.5-3.65	2000+
$LiCoO_2$	LCO	150-240	3.0-4.2	500-1000
$LiMn_2O_4$	LMO	100-150	3.0-4.2	300-700
$LiNiMnCoO_2$	NMC	150-220	3.0-4.2	1000-2000
$LiNiCoAlO_2$	NCA	200-260	3.0-4.2	500
Li_2TiO_3	LTO	50-80	1.8-2.85	3000-7000
Lead-Acid	LA	30-40	1.8-2.3	200-1500

Table 5.1: Battery types and their different characteristics [37], [41]

Energy density, defined as the amount of energy stored per unit volume or mass, is a crucial metric for battery performance. LIBs exhibit superior energy density compared to traditional

battery technologies such as Nickel-Cadmium (Ni-Cd) or lead-acid batteries. Modern LIBs can achieve energy densities up to 260 $\frac{\text{Wh}}{\text{kg}}$ at a voltage of 4.2 V, driven by advancements in materials and cell design. Table 5.1 provides a breakdown of the different battery technologies and their performance.

The high energy density of LIBs is attributed to the use of lithium, the lightest metal with the highest electrochemical potential. This characteristic enables LIBs to store more energy in a compact and lightweight package, making them ideal for portable and mobile applications [42].

5.2.2.2 Innovations in Lithium-Ion Batteries

Several key innovations have propelled the development of LIBs, enhancing their performance, safety, and application range. The development of high-capacity cathode materials like Lithium Cobalt Oxide ($LiCoO_2$), Nickel Manganese Cobalt (NMC), and Lithium Iron Phosphate ($LiFePO_4$) has been pivotal. These materials offer improved energy density, cycle life, and thermal stability [43]. Innovations in anode materials, including the use of graphite and silicon alloys, have also significantly increased capacity and reduced charging times [44].

Advancements in electrolyte formulations have also enhanced the safety and performance of LIBs. Functional electrolytes containing additives such as vinylene carbonate and fluoroethylene carbonate form a stable solid electrolyte interphase (SEI) on the anode, preventing electrolyte decomposition and extending battery life. Fire-retardant additives and improved wetting agents have also been developed to enhance safety and performance [45].

Improvements in cell design, including the development of prismatic, cylindrical, and pouch cell formats, have optimized the energy density and manufacturability of LIBs. High-speed automated production processes have reduced costs and improved quality control, making LIBs more affordable and reliable [46].

5.2.2.3 Benefits of Lithium-Ion Batteries

LIBs offer the highest energy density among commercially available rechargeable batteries, enabling longer runtime for portable devices and greater range for electric vehicles. They can also endure hundreds to thousands of charge-discharge cycles, making them cost-effective over their lifespan. Their low self-discharge rate makes them ideal for applications where frequent charging is not possible; they retain their charge better than other rechargeable batteries when not in use.

5.2.2.4 Drawbacks of Lithium-Ion Batteries

Though rare, lithium-ion batteries are susceptible to thermal runaway, leading to overheating and potential explosions if not properly managed. This necessitates robust battery management systems (BMS) to monitor and control charging and discharging processes. The manufacturing processes and materials for LIBs are expensive, making them costlier than other rechargeable battery technologies. This being said, due to the scale of lithium-ion manufacturing demands, these costs are quickly coming down, making them more affordable and accessible [47].

5.2.2.5 Implications for the Hybrid Vehicle

Lithium-Ion batteries represent a significant advancement in energy storage technology, characterized by high energy density and robust performance. Innovations in materials, electrolytes, and manufacturing processes have continued to improve their safety, efficiency, and application range. However, challenges such as safety concerns, high costs, environmental impacts, and performance under extreme conditions need to be addressed to fully realize their potential in future energy solutions.

5.3 Sizing the Battery Pack *Without* Regenerative Braking

In this section, energy and battery estimates are presented assuming no energy would be recovered through regenerative braking. Section 5.4 discusses how the battery can actually be quite a bit smaller if a certain amount of energy recuperation is assumed.

5.3.1 Energy Requirements for the Battery Pack *Without* Regenerative Braking

To determine the energy requirements of the vehicle without accounting for regenerative braking, it was assumed that the electric motor would be utilized for 30 seconds per lap over a total of 25 consecutive laps. During these periods, the electric motor was estimated to operate at peak power P_E^{Peak} for 50% of the time and at continuous power P_E^{Cont} for the remaining 50% of the time, as defined in Table 6.2. Thus, the nominal power of the electric motor for a given lap was estimated to be 37.5 kW (5.1).

$$\begin{aligned} P_E^{\text{Nominal}} &= \left[\%^{Cont} \times P_E^{Cont}\right] + \left[\%^{Peak} \times P_E^{Peak}\right] \\ P_E^{\text{Nominal}} &= [50\% \times 20 \text{ kW}] + [50\% \times 55 \text{ kW}] \\ P_E^{\text{Nominal}} &= 37.5 \text{ kW} \end{aligned} \tag{5.1}$$

Therefore, the total energy consumed during a single lap of a race is approximated to be 0.3125 kWh according to equation (5.2).

$$\begin{aligned} E_{\text{Lap}}^{\text{No Regen}} &= P_E^{\text{Nominal}} \times \text{Time On per Lap} \\ E_{\text{Lap}}^{\text{No Regen}} &= 37.5 \text{ kW} \times 30 \ \frac{\text{sec}}{\text{Lap}} \\ E_{\text{Lap}}^{\text{No Regen}} &= 0.3125 \text{ kWh} \end{aligned} \tag{5.2}$$

With this information, the total energy consumption during a race is approximated to be 7.8125 kWh according to equation (5.3).

$$\begin{aligned} E_{\text{Race}}^{\text{No Regen}} &= E_{\text{Lap}} \times \text{Number of Laps} \\ E_{\text{Race}}^{\text{No Regen}} &= P_E^{\text{Nominal}} \times \text{Time On per Lap} \times \text{Number of Laps} \\ E_{\text{Race}}^{\text{No Regen}} &= 37.5 \text{ kW} \times 30 \ \frac{\text{sec}}{\text{Lap}} \times 25 \text{ Laps} \\ E_{\text{Race}}^{\text{No Regen}} &= 7.8125 \text{ kWh} \end{aligned} \tag{5.3}$$

Using equation (5.4), the mass of the battery can be estimated from the energy required and the energy mass density of the battery technology.

$$M_{\text{Batt}} = E_{\text{Race}}^{\text{No Regen}} \times \text{Energy Mass Density} \tag{5.4}$$

5.3.2 Battery Masses for Different Cell Chemistries *Without* Regenerative Braking

Using equation (5.4), Table 5.2 determines the battery masses for a variety of different battery types. The data presented in the table showcases the relationship between energy mass density and the corresponding battery mass for various battery chemistries. This table is pivotal for understanding the trade-offs between different battery technologies, especially in applications requiring specific energy capacities and weight constraints.

Battery Type	Energy Mass Density $\left[\frac{\text{Wh}}{\text{kg}}\right]$	Battery Mass [kg]
LiFePO$_4$ (LFP)	90	86.81
LiFePO$_4$ (LFP)	105	74.40
LiFePO$_4$ (LFP)	120	65.10
LiCoO$_2$ (LCO)	150	52.08
LiCoO$_2$ (LCO)	195	40.06
LiCoO$_2$ (LCO)	240	32.55
LiNiCoAlO$_2$ (NCA)	200	39.06
LiNiCoAlO$_2$ (NCA)	230	33.97
LiNiCoAlO$_2$ (NCA)	260	30.05
Lead-Acid	30	260.42
Lead-Acid	35	223.21
Lead-Acid	40	195.31

Table 5.2: Battery Technology and Associated Mass for a 7.8125 kWh Battery

Overall, the data in Table 5.2 underscores the advantages of energy-dense batteries in reducing the overall weight of energy storage systems. This reduction in weight can lead to enhanced efficiency and performance, especially for a racecar.

5.4   Sizing the Battery Pack *With* Regenerative Braking

In this section, energy and battery estimates are presented assuming that some energy would be recovered through regenerative braking. Section 5.3 discusses how the battery can actually be quite a bit smaller if a certain amount of energy recuperation is assumed.

5.4.1   Energy Requirements for the Battery Pack *With* Regenerative Braking

To determine the energy requirements of the vehicle assuming that some energy will be recovered during the race through regenerative braking, the values computed in Section 4.3.4 were used. As presented in Tables 4.1 and 4.2, the average amount of energy recovered during a single lap of a race at Palmer Motorsports Park and the Podium Club Racetrack was approximately 168.80 Wh and 189.43 Wh, respectively. P_E^{Nominal} computed in section 5.1 will be used, as regenerative braking does not influence the peak power of the vehicle. Therefore, it is assumed that an average of 179.115 Wh is recovered per lap through regenerative braking, as shown in equation (5.5).

$$\text{Energy Recovered Per Lap} = \frac{168.80 \text{ Wh} + 189.43 \text{ Wh}}{2} = 179.115 \text{ Wh} \qquad (5.5)$$

The total energy consumed during a single lap of a race with regenerative braking is approximated to be 0.1334 kWh according to equation (5.6).

$$
\begin{aligned}
E_{\text{Lap}}^{\text{Regen}} &= \left[P_E^{\text{Nominal}} \times \text{Time On per Lap} \right] - \text{Energy Recovered Per Lap} \\
E_{\text{Lap}}^{\text{Regen}} &= \left[37.5 \text{ kW} \times 30 \, \frac{\text{sec}}{\text{Lap}} \right] - [0.179115 \text{ kWh}] \\
E_{\text{Lap}}^{\text{Regen}} &= 0.1334 \text{ kWh}
\end{aligned}
\qquad (5.6)
$$

Therefore, the total energy consumed during a race when regenerative braking is enabled is approximated to be 3.335 kWh (5.7).

$$
\begin{aligned}
E_{\text{Race}}^{\text{Regen}} &= \left[\left(P_E^{\text{Nominal}} \times \text{Time On per Lap} \right) - (E_{Regen}) \right] \times \text{Number of Laps} \\
E_{\text{Race}}^{\text{Regen}} &= \left[\left(37.5 \text{ kW} \times 30 \, \frac{\text{sec}}{\text{Lap}} \right) - (0.17912 \text{ kWh}) \right] \times 25 \text{ Laps} \\
E_{\text{Race}}^{\text{Regen}} &= 3.335 \text{ kWh}
\end{aligned}
\qquad (5.7)
$$

Using equation (5.8), the mass of the battery can be estimated from the energy required and the energy mass density of the battery technology.

$$M_{\text{Batt}} = E_{\text{Race}}^{\text{Regen}} \times \text{Energy Mass Density} \qquad (5.8)$$

5.4.2 Battery Masses for Different Cell Chemistries *With* Regenerative Braking

Using equation (5.8), Table 5.3 determines the battery masses for a variety of different battery types when regnerative braking is assumed.

Overall, the data in Table 5.3 underscores the advantages of energy-dense batteries in reducing the overall weight of energy storage systems. This reduction in weight can lead to enhanced efficiency and performance, especially for a racecar. There is also a significant weight reduction when compared to the non-regenerative braking case presented in Table 5.2.

As battery technology continues to evolve, focusing on increasing energy mass density will be crucial for developing lighter and more efficient energy storage solutions. The comparison

Battery Type	Energy Mass Density $\left[\frac{Wh}{kg}\right]$	Battery Mass [kg]
LiFePO$_4$ (LFP)	90	37.05
LiFePO$_4$ (LFP)	105	31.76
LiFePO$_4$ (LFP)	120	27.79
LiCoO$_2$ (LCO)	150	22.23
LiCoO$_2$ (LCO)	195	17.10
LiCoO$_2$ (LCO)	240	13.89
LiNiCoAlO$_2$ (NCA)	200	16.67
LiNiCoAlO$_2$ (NCA)	230	14.50
LiNiCoAlO$_2$ (NCA)	260	12.83
Lead-Acid	30	111.15
Lead-Acid	35	95.27
Lead-Acid	40	83.37

Table 5.3: Battery Technology and Associated Mass for a 3.3335 kWh Battery

also highlights the stark contrast in mass compared between lead-acid batteries and an equivalently sized lithium-based battery. In applications where weight and space are limited, lead-acid batteries become almost completely infeasible.

Chapter 6

Vehicle Calculations and Specifications

This chapter reviews the critical aspects of vehicle calculations and specifications, focusing on the selection and implementation of an electric motor for a hybrid powertrain system. It begins with Section 6.1, discussing the electric motor selection process, weighing the benefits and trade-offs of various motor candidates, and ultimately justifying the choice of the Mot Energy ME1616 motor. Section 6.2 analyzes the performance statistics of the gas-powered RUSH SR, establishing baseline metrics such as torque, torque-to-mass ratio, and power-to-mass ratio. The chapter then transitions to evaluating the performance of the hybrid RUSH SR in Sections 6.3 and 6.4, both without and with regenerative braking, respectively. These sections highlight the substantial improvements in torque-to-mass and power-to-mass ratios achieved through hybridization and energy recovery. This comprehensive analysis underscores the performance benefits and feasibility of implementing a hybrid powertrain system in the RUSH SR vehicle.

6.1 Electric Motor Selection and Specifications

Needless to say, one of the most critical components of a hybrid powertrain system is the electric motor. Section 6.1.1 discusses the benefits and tradeoffs that were made during the selection process of the motor. Section 6.1.2 highlights the key specifications and motor constants for the motor that was ultimately selected.

6.1.1 Electric Motor Selection

Selecting a motor that has high power, low mass, and a reasonable price were significant factors that determined the downselection process from the motor candidates described in Table 6.1.

Table 6.1: Candidate Electric Motors for the Hybrid Conversion [48]–[52]

Motor Name	Mass [kg]	Peak Speed [RPM]	Stall Torque [Nm]	Peak Power [kW]	Power Density [$\frac{kW}{kg}$]	Price [$]
EMRAX 208	10	7,000	150	86	8.60	$6,000
EMRAX 188	7.1	8,000	100	60	8.45	$4,000
NOVA 50	11.5	5,600	142	50	4.35	$5,000
EBMX 80	15	12,000	65	40	2.67	$1,450
ME1616	22	6,000	134	55	2.50	$850

While the EMRAX 188 and 208 have the highest Power Densities at 8.60 $\frac{kW}{kg}$ and 8.45 $\frac{kW}{kg}$ respectively, their prices exceeded the allotted budget RUSH was aiming to achieve with this system. The NOVA 50 was also too expensive, so it was not considered beyond this point.

This leaves the EBMX 80 and the ME1616 as the remaining motor candidates. While the EBMX 80 has a slightly higher power density of 2.67 $\frac{kW}{kg}$ compared to the ME1616's power density of 2.50, the ME1616 was ultimately selected due to its significantly lower price, and greater peak power capabilities. The marginal compromise on power density was worth the other benefits of the ME1616.

6.1.2 Mot Energy ME1616 Electric Motor Specifications

Mot Energy's ME1616 electric motor was ultimately selected, and for the following analyses, the constants defined in Table 1.1 and Table 6.2 were utilized for all computations.

Table 6.2: Mot Energy ME1616 Motor Parameters and Specifications

Parameter	Symbol	Value	Units
Motor Mass	M_E	22	Kilogram [kg]
Continuous Power	P_E^{Cont}	20	Kilowatts [kW]
Peak Power	P_E^{Peak}	55	Kilowatts [kW]
Stall Torque	τ_E^{Stall}	134	Newton Meters [Nm]
Continuous Torque	τ_E^{Cont}	55	Newton Meters [Nm] (at 250 A)
Peak Rotor Speed	ω_E	6,000	Revolutions per Minute [RPM]
Continuous Current	I_{Cont}	250	Amps [A]
Peak Current	I_{Peak}	600	Amps [A] (1 minute)

6.2 Baseline Performance Statistics for the Gas-Powered RUSH SR

This section discusses key performance statistics for the entirely gas-powered RUSH SR. These baselines help quantify the current performance of the RUSH SR, and allow us to estimate whether or not significant performance gains could be achieved by implementing the hybrid powertrain system.

6.2.1 Torque

The Power of the gas-powered RUSH SR can be determined using equation (6.1).

$$P = \tau \times \omega$$
$$P_{Gas} = \tau \times \omega_{Gas}^{Motor}$$
(6.1)

P is the power in watts, τ is the torque in newton meters, and ω is the angular speed in radians per second $\frac{rad}{sec}$.

Using this equation, we can determine the torque τ of the system by simply rearranging the equation, as exhibited in equation (6.2).

$$\tau = \frac{P}{\omega}$$
$$\tau = \frac{P_{Gas}}{\omega_{Gas}^{Motor}}$$
(6.2)

τ is the torque in newton meters, P is the power in watts, and ω is the angular speed in radians per second $\frac{rad}{sec}$.

The final component we need to determine the torque of the gas-powered vehicle is the angular acceleration ω of the gas motor. Using the RPM of the gas motor, the angular acceleration of the vehicle with the gas motor can be determined using equation (6.3).

$$\omega = \text{RPM} \times \frac{2\pi}{60}$$
$$\omega = 11,800 \times \frac{2\pi}{60}$$
$$\omega = 1235.69 \, \frac{rad}{sec}$$
(6.3)

Utilizing the vehicle and motor constants included in Tables 1.1 and 6.2, the gas vehicle's torque output is estimated to be 87.503 Nm (6.4).

$$\tau_{\text{Gas}} = \frac{P_{Gas}}{\omega}$$
$$\tau_{\text{Gas}} = 87.503 \, \text{Nm}$$

$$(6.4)$$

6.2.2 Torque-to-Mass Ratio of the Gas-Powered Vehicle

Given this baseline torque value $\tau_{\text{Gas}} = 87.503 \, \text{Nm}$ for the gas-powered vehicle, we find that the RUSH SR in its current, unmodified configuration has a Torque-to-Mass Ratio (TMR) of approximately $0.171 \, \frac{\text{Nm}}{\text{kg}}$ (6.5).

$$\text{TMR}_{\text{Gas}} = \frac{\tau_{\text{Gas}}}{M_V}$$
$$\text{TMR}_{\text{Gas}} = \frac{87.503 \, \text{Nm}}{513 \, \text{kg}}$$
$$\text{TMR}_{\text{Gas}} = 0.171 \, \frac{\text{Nm}}{\text{kg}}$$

$$(6.5)$$

6.2.3 Power-to-Mass Ratio of the Gas-Powered Vehicle

The Power-to-Mass ratio is another key baseline parameter used to evaluate the performance of vehicles. Like TMR, maximizing this value is critical to deliver high performance during a race. Using the baseline power value $P_{\text{Gas}} = 108.13 \, \text{kW}$ for the gas-powered vehicle, we find that the RUSH SR in its current, unmodified configuration has a Power-to-Mass Ratio (PMR) of approximately $210.77 \, \frac{\text{Watts}}{\text{kg}}$ (6.6).

$$\text{PMR}_{\text{Gas}} = \frac{P_{\text{Gas}}}{M_V}$$
$$\text{PMR}_{\text{Gas}} = \frac{108,130 \, \text{Watts}}{513 \, \text{kg}}$$
$$\text{PMR}_{\text{Gas}} = 210.77 \, \frac{\text{Watts}}{\text{kg}}$$

$$(6.6)$$

6.3 Performance Statistics for the Hybrid RUSH SR *Without* Regenerative Braking

6.3.1 Torque

Similar to how P_E^{Nominal} was calculated for the electric vehicle using equation 5.1, the nominal torque τ_E^{Nominal} can be similarly calculated using equation (6.7).

$$
\begin{aligned}
\tau_E^{\text{Nominal}} &= \left[\%^{Cont} \times \tau_E^{Cont}\right] + \left[\%^{Peak} \times \tau_E^{Stall}\right] \\
\tau_E^{\text{Nominal}} &= [50\% \times 55 \text{ Nm}] + [50\% \times 134 \text{ Nm}] \\
\tau_E^{\text{Nominal}} &= 94.5 \text{ Nm}
\end{aligned}
\tag{6.7}
$$

As a result, the hybrid vehicle's nominal torque is estimated to be $\tau_{\text{Hybrid}} = 182.003$ Nm, over double $\tau_{\text{Gas}} = 87.503$ Nm (6.8).

$$
\begin{aligned}
\tau_{\text{Hybrid}} &= \tau_{\text{Gas}} + \tau_E^{\text{Nominal}} \\
\tau_{\text{Hybrid}} &= 85.503 \text{ Nm} + 94.5 \text{ Nm} \\
\tau_{\text{Hybrid}} &= 182.003 \text{ Nm}
\end{aligned}
\tag{6.8}
$$

6.3.2 Torque-to-Mass Ratio *Without* Regenerative Braking

Due to the fact that there are many battery options available for consideration for this hybrid conversion project, it would be irresponsible to calculate a single Torque-to-Mass ratio for the hybrid vehicle, as these parameters are constantly changing and no actual battery selection has been made yet. Therefore, the torque-to-mass ratio of the hybrid vehicle without any regenerative braking is calculated multiple times for each battery technology under consideration, with the minimum, average, and maximum cell energy mass density being evaluated, as shown in Table 6.3. These values were calculated according to equation (6.9)

$$
\text{TMR}_{\text{Hybrid}} = \frac{\tau_{\text{Gas}} + \tau_{\text{Hybrid}}}{M_V + M_{Batt} + M_E}
\tag{6.9}
$$

Recall that from Section 6.2.2, the gas-powered vehicle had a torque-to-mass ratio of approximately $\text{TMR}_{\text{Gas}} = 0.171 \frac{\text{Nm}}{\text{kg}}$. *All* torque-to-mass ratios for the hybrid vehicle are greater than this, indicating that any hybrid configuration using the ME1616 motor would lead to

Battery Type	Energy Mass Density $\left[\frac{\text{Wh}}{\text{kg}}\right]$	Battery Mass [kg]	Torque-to-Mass Ratio $\left[\frac{\text{Nm}}{\text{kg}}\right]$	Torque-to-Mass Improvement [%]
Gas-Powered RUSH SR			0.171	
LiFePO$_4$ (LFP)	90	86.81	0.384	+ 125.13%
LiFePO$_4$ (LFP)	105	74.40	0.391	+ 129.19%
LiFePO$_4$ (LFP)	120	65.10	0.396	+ 132.32%
LiCoO$_2$ (LCO)	150	52.08	0.404	+ 136.86%
LiCoO$_2$ (LCO)	195	40.06	0.411	+ 141.20%
LiCoO$_2$ (LCO)	240	32.55	0.416	+ 144.00%
LiNiCoAlO$_2$ (NCA)	200	39.06	0.412	+ 141.57%
LiNiCoAlO$_2$ (NCA)	230	33.97	0.415	+ 143.47%
LiNiCoAlO$_2$ (NCA)	260	30.05	0.418	+ 144.95%
Lead-Acid	30	260.42	0.308	+ 80.49%
Lead-Acid	35	223.21	0.322	+ 88.50%
Lead-Acid	40	195.31	0.333	+ 94.99%

Table 6.3: Torque-to-Mass Ratios for All Considered Battery Technologies *Without* Regenerative Braking

performance gains (even an entirely lead-acid battery system, which would be ridiculous and impractical).

6.3.3 Power-to-Mass Ratio *Without* Regenerative Braking

Like the torque-to-mass ratio computations performed in section 6.3.2, to accurately gauge the performance trade-offs of a hybrid powertrain system, it would be best to consider all of the battery options available, as a battery technology has not yet been selected. Therefore, the power-to-mass ratio of the hybrid vehicle is calculated multiple times for each battery technology being considered, with the minimum, average, and maximum cell energy mass density cases evaluated, as shown in Table 6.4. These values were calculated according to equation (6.10).

$$\text{PMR}_{\text{Hybrid}} = \frac{P_{\text{Gas}} + P_{\text{Hybrid}}}{M_V + M_{Batt} + M_E} \tag{6.10}$$

Unlike the torque-to-mass ratio discussed in Section 6.3.2, the hybrid system does not outperform the ICE system in *all* cases. In all *practical* cases, however, the hybrid power-to-mass ratio is greater than the gas-powered power-to-mass ratio.

Battery Type	Energy Mass Density $\left[\frac{\text{Wh}}{\text{kg}}\right]$	Battery Mass [kg]	Power-to-Mass Ratio $\left[\frac{\text{W}}{\text{kg}}\right]$	Power-to-Mass Improvement [%]
Gas-Powered RUSH SR			210.77	
LiFePO$_4$ (LFP)	90	86.81	207.50	$-$ 1.55%
LiFePO$_4$ (LFP)	105	74.40	211.24	$+$ 0.22%
LiFePO$_4$ (LFP)	120	65.10	214.12	$+$ 1.59%
LiCoO$_2$ (LCO)	150	52.08	218.30	$+$ 3.57%
LiCoO$_2$ (LCO)	195	40.06	222.31	$+$ 5.47%
LiCoO$_2$ (LCO)	240	32.55	224.89	$+$ 6.70%
LiNiCoAlO$_2$ (NCA)	200	39.06	222.65	$+$ 5.63%
LiNiCoAlO$_2$ (NCA)	230	33.97	224.40	$+$ 6.46%
LiNiCoAlO$_2$ (NCA)	260	30.05	225.76	$+$ 7.11%
Lead-Acid	30	260.42	166.35	$-$ 21.08%
Lead-Acid	35	223.21	173.73	$-$ 17.57%
Lead-Acid	40	195.31	179.72	$-$ 14.73%

Table 6.4: Power-to-Mass Ratios for All Considered Battery Technologies *Without* Regenerative Braking

Recall that from Section 6.2.3, the gas-powered vehicle had a power-to-mass ratio of approximately $\text{PMR}_{\text{Gas}} = 210.77 \frac{\text{W}}{\text{kg}}$. Except for the most conservative LiFePO$_4$ (LFP) case, where the energy mass density is assumed to be the minimum of $90 \frac{\text{Wh}}{\text{kg}}$, all other lithium-ion battery technologies would lead to the hybrid vehicle having a higher overall power-to-mass ratio. Even in this case, the power-to-mass ratio was $207.50 \frac{\text{W}}{\text{kg}}$, a 1.55% decrease from the original PMR_{Gas}.

Needless to say, an entirely lead-acid battery would perform significantly worse due to its very heavy weight, but this battery technology was included to demonstrate how energy dense lithium-ion batteries are, not to demonstrate that the vehicle should use lead-acid batteries.

Overall, the analysis in this section provides quantitative evidence supporting the implementation of a hybrid powertrain system, even without any form of energy recovery. Such a system would lead to noticeable and significant improvements in the power-to-mass ratio of the vehicle, and would nearly double the torque-to-mass ratio of the vehicle.

6.4 Performance Statistics for the Hybrid RUSH SR *With* Regenerative Braking

When the RUSH SR is considered to have regenerative braking capabilities, a certain portion of the kinetic energy typically dissipated as heat energy can instead be recovered and used to recharge the vehicle's batteries. As discussed in Section 4.3.1, approximately $\eta_{Regen} = 25\%$ of this braking energy can be converted into electrical energy. For the following analyses, it is assumed that 25% of the energy dissipated during braking is recovered.

Without regenerative braking, the vehicle required a 7.8125 kWh battery pack in order to hit the performance targets looking to be achieved. *With* regenerative braking, however, the required battery size shrinks to 3.3335 kWh, approximately 57.33% smaller than the original battery. This leads to significant battery mass savings M_{Batt}, which reduces the vehicle's total mass. As a result, both the torque-to-mass ratio and the power-to-mass ratio are improved for the vehicle with regenerative braking.

6.4.1 Torque-to-Mass Ratio *With* Regenerative Braking

Battery Type	Energy Mass Density $\left[\frac{Wh}{kg}\right]$	Battery Mass [kg]	Torque-to-Mass Ratio $\left[\frac{Nm}{kg}\right]$	Torque-to-Mass Improvement [%]
Gas-Powered RUSH SR			0.171	
LiFePO$_4$ (LFP)	90	37.05	0.413	+ 142.32%
LiFePO$_4$ (LFP)	105	31.76	0.417	+ 144.30%
LiFePO$_4$ (LFP)	120	27.79	0.419	+ 145.81%
LiCoO$_2$ (LCO)	150	22.23	0.423	+ 147.95%
LiCoO$_2$ (LCO)	195	17.10	0.426	+ 149.96%
LiCoO$_2$ (LCO)	240	13.89	0.429	+ 151.24%
LiNiCoAlO$_2$ (NCA)	200	16.67	0.427	+ 150.13%
LiNiCoAlO$_2$ (NCA)	230	14.50	0.428	+ 151.00%
LiNiCoAlO$_2$ (NCA)	260	12.83	0.429	+ 151.67%
Lead-Acid	30	111.15	0.371	+ 117.59%
Lead-Acid	35	95.27	0.379	+ 122.45%
Lead-Acid	40	83.37	0.386	+ 126.25%

Table 6.5: Torque-to-Mass Ratios for All Considered Battery Technologies *With* Regenerative Braking

With the updated battery capacities and masses for the system with regenerative braking,

the process of determining the torque-to-mass-ratio is essentially identical to the process discussed in Section 6.4.1. Like above, the torque-to-mass ratio of the hybrid vehicle with regenerative braking is calculated multiple times for each battery technology, with the minimum, average, and maximum cell energy mass density being evaluated, as shown in Table 6.5. These values were calculated according to equation (6.9).

Since the implementation of a regenerative braking system leads to the battery mass M_{Batt} decreasing, the associated torque-to-mass ratios for the hybrid with regenerative braking are greater than the torque-to-mass ratios for a hybrid without regenerative braking. Increasing the torque-to-mass ratio would enable the vehicle to accelerate much faster, especially at lower speeds. This would enable a vehicle to get up to speed in less time after they had slowed down for a corner.

Recall that from Section 6.2.2, the gas-powered vehicle had a torque-to-mass ratio of approximately $\text{TMR}_{\text{Gas}} = 0.171 \frac{\text{Nm}}{\text{kg}}$. *All* torque-to-mass ratios for the hybrid vehicle are greater than this, indicating that any hybrid configuration using the ME1616 motor would lead to significant performance gains (even an entirely lead-acid battery system, which would be ridiculous and impractical).

6.4.2 Power-to-Mass Ratio *With* Regenerative Braking

Battery Type	Energy Mass Density $\left[\frac{\text{Wh}}{\text{kg}}\right]$	Battery Mass [kg]	Power-to-Mass Ratio $\left[\frac{\text{W}}{\text{kg}}\right]$	Power-to-Mass Improvement [%]
Gas-Powered RUSH SR			210.77	
LiFePO$_4$ (LFP)	90	37.05	223.34	+ 5.96%
LiFePO$_4$ (LFP)	105	31.76	225.16	+ 6.83%
LiFePO$_4$ (LFP)	120	27.79	226.55	+ 7.49%
LiCoO$_2$ (LCO)	150	22.23	228.53	+ 8.42%
LiCoO$_2$ (LCO)	195	17.10	230.38	+ 9.30%
LiCoO$_2$ (LCO)	240	13.89	231.56	+ 9.86%
LiNiCoAlO$_2$ (NCA)	200	16.67	230.54	+ 9.38%
LiNiCoAlO$_2$ (NCA)	230	14.50	231.34	+ 9.76%
LiNiCoAlO$_2$ (NCA)	260	12.83	231.95	+ 10.05%
Lead-Acid	30	111.15	200.54	− 4.85%
Lead-Acid	35	95.27	205.03	− 2.73%
Lead-Acid	40	83.37	208.52	− 1.07%

Table 6.6: Power-to-Mass Ratios for All Considered Battery Technologies *With* Regenerative Braking

Like the torque-to-mass ratio computations performed in Section 6.4.1, the process for the power-to-mass ratio is essentially identical to the process described in Section 6.3.3 for a hybrid with regenerative braking. The power-to-mass ratio of the hybrid vehicle with regenerative braking is calculated multiple times for each battery technology, with the minimum, average, and maximum cell energy mass density cases evaluated, as shown in Table 6.6. These values were calculated according to equation (6.10).

With regenerative braking, the battery mass reductions that can be achieved significantly improve the overall power-to-mass ratio by a substantial margin. *All* lithium-ion battery types at this battery capacity have greater power-to-mass ratios than the original gas-powered vehicle and the non-regenerative braking hybrid vehicle.

As determined in Section 6.2.3, the gas-powered vehicle had a power-to-mass ratio of approximately $\mathrm{PMR_{Gas}} = 210.77 \frac{\mathrm{W}}{\mathrm{kg}}$. Even with the most conservative LiFePO$_4$ (LFP) case (where energy mass density is assumed to be the minimum of $90 \frac{\mathrm{Wh}}{\mathrm{kg}}$), the power-to-mass ratio increases to $223.34 \frac{\mathrm{W}}{\mathrm{kg}}$, a 5.96% improvement from the gas-powered vehicle's power-to-mass ratio.

Using similar battery cells to what Tesla uses in its vehicles (the LiNiCoAlO$_2$ NCA cell), a 10.05% increase in the power-to-mass ratio can be achieved when compared to the gas-powered. This increases the power-to-mass ratio to $231.95 \frac{\mathrm{W}}{\mathrm{kg}}$ from the original value of $210.77 \frac{\mathrm{W}}{\mathrm{kg}}$.

Once again, an entirely lead-acid battery would lead to vehicle performance that is significantly worse than an equally sized lithium-ion battery due to its very heavy weight. This battery technology was included to demonstrate how energy dense lithium-ion batteries are, not to demonstrate that the vehicle should use lead-acid batteries.

Overall, the analysis in this section provides quantitative evidence supporting the implementation of a hybrid powertrain system, especially with a form of energy recovery. Such a system would lead to noticeable and significant improvements in the power-to-mass ratio of the vehicle, and would double the torque-to-mass ratio of the vehicle. These performance improvements would be noticed anytime when the driver presses the accelerator pedal.

Chapter 7

Conclusion

7.1 Key Takeaways

The research presented in this thesis highlights the significant advantages of incorporating regenerative braking systems in electric and hybrid vehicles. One of the primary conclusions is that a hybrid vehicle, despite its heavier mass due to the additional components such as batteries and electric motors, would outperform its gasoline counterpart 6.4.2. This performance superiority is attributed to the efficient utilization of energy and the improved acceleration and braking dynamics offered by hybrid technology.

Chapter 3 and Chapter 4 provided detailed analyses of the gas-powered vehicle's performance throughout different races, and then used this data to estimate the amount of energy that could be recovered during braking using a regenerative braking system. The findings indicated that regenerative braking not only extends the driving range of electric and hybrid vehicles but also improves their performance by providing additional power during acceleration phases. This dual benefit of increased range and enhanced performance underscores the critical role of regenerative braking in modern vehicle design.

The thesis also emphasized the importance of advanced battery technologies in maximizing the benefits of regenerative braking. Chapter 5 outlined how properly sized and efficient batteries are crucial for storing the recuperated energy and making it readily available for use. The integration of these advanced battery systems ensures that the energy recovered during braking is efficiently utilized, thereby boosting the vehicle's performance and overall efficiency.

In conclusion, this thesis underscores that hybrid vehicles, equipped with regenerative braking systems, offer a superior performance profile compared to traditional gasoline vehicles. The ability to recuperate and reuse energy not only mitigates the drawbacks of increased mass but also provides a tangible enhancement in vehicle dynamics. These findings advocate for the broader adoption of regenerative braking systems and advanced battery technologies

in the automotive industry to achieve a more sustainable and high-performing future for electric and hybrid vehicles.

7.2 Chapter Summaries

In this thesis, various aspects of regenerative braking systems in electric vehicles were explored, particularly in the context of motorsports vehicles and the RUSH SR. The bulk of the analysis focused on interpreting vehicle race data, energy recuperation during braking, battery specifications and sizing, and overall vehicle calculations and specifications. Each chapter has contributed to a comprehensive understanding of how regenerative braking can enhance the efficiency and performance of electric vehicles.

Chapter 1 set the stage by highlighting the importance of regenerative braking in electric vehicles. It provided an overview of the current challenges in energy efficiency and the potential benefits of integrating regenerative braking systems. This foundational context underscored the significance of the subsequent chapters' analyses and findings.

Chapter 2 delved into the mechanics and principles of regenerative braking. It explained how kinetic energy, which is typically lost as heat during braking, can be converted back into electrical energy and stored in the vehicle's battery. The analysis covered various regenerative braking technologies and their efficiencies, setting the foundation for further exploration in subsequent chapters.

In Chapter 3, race data was analyzed to understand the performance of vehicles equipped with regenerative braking systems. By examining parameters such as speed, braking instances, and energy consumption, it was possible to identify patterns and potential areas for improvement in energy recuperation strategies. The data indicated that significant energy savings could be achieved, particularly in high-frequency braking scenarios.

Building on the race data analysis, Chapter 4 estimated the amount of energy that could be recuperated during braking events. By applying mathematical models and simulation techniques, it was shown that energy recuperation could contribute substantially to extending the range of electric vehicles. This chapter also highlighted the factors affecting energy recuperation efficiency, such as vehicle speed and braking force.

Chapter 5 focused on the battery technology necessary to support regenerative braking. It detailed the specifications and sizing requirements for batteries to efficiently store the recuperated energy. The analysis included considerations for battery capacity, charging rates, and thermal management, emphasizing the need for advanced battery systems to maximize the benefits of regenerative braking.

The final analytical chapter, Chapter 6, brought together the findings from previous sections to present comprehensive vehicle calculations and specifications. It integrated data on energy

recuperation, battery capacity, and vehicle performance to propose optimal configurations for electric vehicles with regenerative braking systems. This holistic approach demonstrated how various components must work in harmony to achieve maximum efficiency.

7.3   Future Work

While this thesis has provided significant insights into regenerative braking systems, several areas warrant further research and development to enhance the findings.

Future work could involve the development of more sophisticated simulation models that account for a wider range of variables, including different driving conditions, vehicle types, and braking strategies. These models could provide more accurate predictions of energy recuperation potential and system performance, thereby enabling more precise optimization of regenerative braking systems.

Continued advancements in battery technology, including the development of higher capacity, faster charging, and more thermally stable batteries, are crucial. Future studies could investigate new battery chemistries and materials that enhance the efficiency and lifespan of batteries used in regenerative braking systems. Such advancements would directly contribute to the overall performance and reliability of electric vehicles.

Implementing regenerative braking systems in real-world scenarios and collecting data over extended periods could provide valuable insights. Long-term studies could help validate simulation models and uncover practical challenges and solutions, ensuring that theoretical findings translate effectively into real-world applications.

A comprehensive cost-benefit analysis considering the economic implications of regenerative braking systems, including initial costs, maintenance, and potential savings, would be beneficial. This analysis could help in understanding the overall financial viability and impact on the market adoption of these technologies. By addressing these areas, future research can build on the findings of this thesis to further enhance the efficiency, performance, and adoption of regenerative braking systems in electric vehicles, contributing to a more sustainable automotive industry.

References

[1] L. Butcher, "The RUSH of Racing," English, *Racecar Engineering*, vol. 30, no. 3, pp. 14–20, Mar. 2020. URL: https://img1.wsimg.com/blobby/go/5addd696-3a68-4d6f-968e-d7b6dde2003f/downloads/Race%20Car%20Engineering%20Rush%20Article.pdf?ver=1706940958450.

[2] RUSH Auto Works, *RUSH SR - Side Image*. URL: https://rushautoworks.com/wp-content/uploads/2022/12/RAW-SR-Side-Front-e1672687288772.jpg.

[3] C. Yang, T. Sun, W. Wang, Y. Li, Y. Zhang, and M. Zha, "Regenerative braking system development and perspectives for electric vehicles: An overview," *Renewable and Sustainable Energy Reviews*, vol. 198, p. 114 389, Jul. 2024, ISSN: 1364-0321. DOI: 10.1016/j.rser.2024.114389. URL: https://www.sciencedirect.com/science/article/pii/S1364032124001126.

[4] J. K. Ahn, K. H. Jung, D. H. Kim, H. B. Jin, H. S. Kim, and S. H. Hwang, "Analysis of a regenerative braking system for Hybrid Electric Vehicles using an Electro-Mechanical Brake," en, *International Journal of Automotive Technology*, vol. 10, no. 2, pp. 229–234, Apr. 2009, ISSN: 1976-3832. DOI: 10.1007/s12239-009-0027-z. URL: https://doi.org/10.1007/s12239-009-0027-z.

[5] B. Wang, X. Huang, J. Wang, X. Guo, and X. Zhu, "A robust wheel slip ratio control design combining hydraulic and regenerative braking systems for in-wheel-motors-driven electric Vehicles," *Journal of the Franklin Institute*, Special Issue on Control and Estimation of Electrified vehicles, vol. 352, no. 2, pp. 577–602, Feb. 2015, ISSN: 0016-0032. DOI: 10.1016/j.jfranklin.2014.06.004. URL: https://www.sciencedirect.com/science/article/pii/S0016003214001756.

[6] L. Li, X. Li, X. Wang, J. Song, K. He, and C. Li, "Analysis of downshift's improvement to energy efficiency of an electric vehicle during regenerative braking," *Applied Energy*, vol. 176, pp. 125–137, Aug. 2016, ISSN: 0306-2619. DOI: 10.1016/j.apenergy.2016.05.042. URL: https://www.sciencedirect.com/science/article/pii/S0306261916306365.

[7] M. Ehsani, Y. Gao, S. Longo, and K. Ebrahimi, *Modern Electric, Hybrid Electric, and Fuel Cell Vehicles*, 3rd ed. Boca Raton: CRC Press, Mar. 2018, ISBN: 978-0-429-50488-4. DOI: 10.1201/9780429504884. URL: https://doi.org/10.1201/9780429504884.

[8] C. Lv, J. Zhang, Y. Li, and Y. Yuan, "Mechanism analysis and evaluation methodology of regenerative braking contribution to energy efficiency improvement of electrified vehicles," *Energy Conversion and Management*, vol. 92, pp. 469–482, Mar. 2015, ISSN: 0196-8904. DOI: 10.1016/j.enconman.2014.12.092. URL: https://www.sciencedirect.com/science/article/pii/S0196890414011418.

[9] A. T. Hamada and M. F. Orhan, "An overview of regenerative braking systems," *Journal of Energy Storage*, vol. 52, p. 105 033, Aug. 2022, ISSN: 2352-152X. DOI: 10.1016/j.est.2022.105033. URL: https://www.sciencedirect.com/science/article/pii/S2352152X22010350.

[10] N. Feng, J. Yong, and Z. Zhan, "A direct multiple shooting method to improve vehicle handling and stability for four hub-wheel-drive electric vehicle during regenerative braking," en, *Proceedings of the Institution of Mechanical Engineers, Part D: Journal of Automobile Engineering*, vol. 234, no. 4, pp. 1047–1056, Mar. 2020, Publisher: IMECHE, ISSN: 0954-4070. DOI: 10.1177/0954407019867510. URL: https://doi.org/10.1177/0954407019867510.

[11] M. Faraday, "Experimental researches in electricity," *Philosophical Transactions of the Royal Society of London*, vol. 122, pp. 125–162, Dec. 1832, Publisher: Royal Society, ISSN: 0261-0523, 2053-9223. DOI: 10.1098/rstl.1832.0006. URL: https://royalsocietypublishing.org/doi/10.1098/rstl.1832.0006.

[12] C. Geng, D. Ning, L. Guo, Q. Xue, and S. Mei, "Simulation Research on Regenerative Braking Control Strategy of Hybrid Electric Vehicle," en, *Energies*, vol. 14, no. 8, p. 2202, Jan. 2021, Number: 8 Publisher: Multidisciplinary Digital Publishing Institute, ISSN: 1996-1073. DOI: 10.3390/en14082202. URL: https://www.mdpi.com/1996-1073/14/8/2202.

[13] J. Ko, S. Ko, H. Son, B. Yoo, J. Cheon, and H. Kim, "Development of Brake System and Regenerative Braking Cooperative Control Algorithm for Automatic-Transmission-Based Hybrid Electric Vehicles," *IEEE Transactions on Vehicular Technology*, vol. 64, no. 2, pp. 431–440, Feb. 2015, ISSN: 0018-9545, 1939-9359. DOI: 10.1109/TVT.2014.2325056. URL: https://ieeexplore.ieee.org/document/6819438/.

[14] C. Qiu and G. Wang, "New evaluation methodology of regenerative braking contribution to energy efficiency improvement of electric vehicles," *Energy Conversion and Management*, vol. 119, pp. 389–398, Jul. 2016, ISSN: 0196-8904. DOI: 10.1016/j.enconman.2016.04.044. URL: https://www.sciencedirect.com/science/article/pii/S0196890416302941.

[15] E. Lenz, "Ueber die Bestimmung der Richtung der durch elektrodynamische Vertheilung erregten galvanischen Ströme," en, *Annalen der Physik*, vol. 107, no. 31, pp. 483–494, 1834, ISSN: 1521-3889. DOI: 10.1002/andp.18341073103. URL: https://onlinelibrary.wiley.com/doi/abs/10.1002/andp.18341073103.

[16] W. Zhao, G. Wu, C. Wang, L. Yu, and Y. Li, "Energy transfer and utilization efficiency of regenerative braking with hybrid energy storage system," *Journal of Power Sources*, vol. 427, pp. 174–183, Jul. 2019, ISSN: 0378-7753. DOI: 10.1016/j.jpowsour.2019.04.083. URL: https://www.sciencedirect.com/science/article/pii/S037877531930494X.

[17]   X. Zhou, G. Wu, C. Wang, R. Zhang, S. Shi, and W. Zhao, "Cooperative optimization of energy recovery and braking feel based on vehicle speed prediction under downshifting conditions," *Energy*, p. 131 699, May 2024, ISSN: 0360-5442. DOI: 10.1016/j.energy.2024.131699. URL: https://www.sciencedirect.com/science/article/pii/S0360544224014725.

[18]   C. Wang, W. Zhao, and W. Li, "Braking sense consistency strategy of electro-hydraulic composite braking system," *Mechanical Systems and Signal Processing*, vol. 109, pp. 196–219, Sep. 2018, ISSN: 0888-3270. DOI: 10.1016/j.ymssp.2018.02.047. URL: https://www.sciencedirect.com/science/article/pii/S0888327018301110.

[19]   J. P. Joule, "On the effects of magnetism upon the dimensions of iron and steel bars," *The London, Edinburgh, and Dublin Philosophical Magazine and Journal of Science*, vol. 30, no. 199, pp. 76–87, Feb. 1847, ISSN: 1941-5966. DOI: 10.1080/14786444708645656. URL: https://doi.org/10.1080/14786444708645656.

[20]   T. Liu, W. Tan, X. Tang, J. Zhang, Y. Xing, and D. Cao, "Driving conditions-driven energy management strategies for hybrid electric vehicles: A review," *Renewable and Sustainable Energy Reviews*, vol. 151, p. 111 521, Nov. 2021, ISSN: 1364-0321. DOI: 10.1016/j.rser.2021.111521. URL: https://www.sciencedirect.com/science/article/pii/S1364032121007991.

[21]   Palmer Motorsports Park, *Palmer Motorsports Park - Track Information*, English, 2013. URL: https://www.palmermotorsportspark.com/trackinfo.aspx.

[22]   Palmer Motorsports Park, *Palmer Motorsports Park - Track History*, English, 2014. URL: https://palmermotorsportspark.com/trackinfo.aspx?id=div1.

[23]   Podium Club, *Podium Club - Roadcourse*, en, 2024. URL: https://www.podiumclub.com/roadcourse.

[24]   I. Newton, *Philosophiæ Naturalis Principia Mathematica: The Mathematical Principles of Natural Philosophy*, en, trans. by A. Motte. D. Adee, Jul. 1687, ISBN: 978-1-5329-4968-5. URL: https://tile.loc.gov/storage-services/public/gdcmassbookdig/newtonsprincipia00newt_0/newtonsprincipia00newt_0.pdf.

[25]   K. T. Chau, *Alternative Fuels and Advanced Vehicle Technologies for Improved Environmental Performance*, English, R. Folkson, Ed. Woodhead Publishing, Jan. 2014, ISBN: 978-0-85709-522-0. DOI: 10.1533/9780857097422.3.655. URL: https://www.sciencedirect.com/science/article/pii/B9780857095220500212.

[26]   V. Totev and V. Gueorgiev, "Efficiency of Regenerative Braking in Electric Vehicles," English, in *2020 21st International Symposium on Electrical Apparatus & Technologies (SIELA)*, Bourgas, Bulgaria: IEEE, Jun. 2020, pp. 1–4, ISBN: 978-1-72814-346-0. DOI: 10.1109/SIELA49118.2020.9167153. URL: https://ieeexplore.ieee.org/document/9167153.

[27]   S. Heydari, P. Fajri, R. Sabzehgar, and A. Asrari, "Optimal Brake Allocation in Electric Vehicles for Maximizing Energy Harvesting During Braking," English, *IEEE Transactions on Energy Conversion*, vol. 35, no. 4, pp. 1806–1814, Dec. 2020, Conference Name: IEEE Transactions on Energy Conversion, ISSN: 1558-0059. DOI: 10.1109/TEC.2020.2994520. URL: https://ieeexplore.ieee.org/abstract/document/9093163.

[28] G. Pongnot, C. Mayet, and D. Labrousse, "Comparison of Different Braking Strategies to Improve the Energy Recovery of an Electric Vehicle Based on Cascaded H-Bridge Inverter with Batteries," English, in *2023 IEEE Vehicle Power and Propulsion Conference (VPPC)*, ISSN: 2769-4186, IEEE, Oct. 2023, pp. 1–6, ISBN: 979-8-3503-4445-5. DOI: 10.1109/VPPC60535.2023.10403284. URL: https://ieeexplore.ieee.org/document/10403284.

[29] A. Volta, "On the electricity excited by the mere contact of conducting substances of different kinds. In a letter from Mr. Alexander Volta, F. R. S. Professor of Natural Philosophy in the University of Pavia, to the Rt. Hon. Sir Joseph Banks, Bart. K.B. P. R. S," *Philosophical Transactions of the Royal Society of London*, vol. 90, pp. 403–431, Jan. 1800, Publisher: Royal Society, ISSN: 2053-9223. DOI: 10.1098/rstl.1800.0018. URL: https://royalsocietypublishing.org/doi/10.1098/rstl.1800.0018.

[30] P. P. Lopes and V. R. Stamenkovic, "Past, present, and future of lead–acid batteries," English, *Science*, vol. 369, no. 6506, pp. 923–924, Aug. 2020, Publisher: American Association for the Advancement of Science. DOI: 10.1126/science.abd3352. URL: https://www.science.org/doi/full/10.1126/science.abd3352.

[31] Y. Miao, P. Hynan, A. von Jouanne, and A. Yokochi, "Current Li-Ion Battery Technologies in Electric Vehicles and Opportunities for Advancements," en, *Energies*, vol. 12, no. 6, p. 1074, Jan. 2019, Number: 6 Publisher: Multidisciplinary Digital Publishing Institute, ISSN: 1996-1073. DOI: 10.3390/en12061074. URL: https://www.mdpi.com/1996-1073/12/6/1074.

[32] G. Gutmann, "APPLICATIONS - TRANSPORTATION | Electric Vehicle: Batteries," in *Encyclopedia of Electrochemical Power Sources*, J. Garche, Ed., vol. 1, Amsterdam: Elsevier, Jan. 2009, pp. 219–235, ISBN: 978-0-444-52745-5. DOI: 10.1016/B978-044452745-5.00087-3. URL: https://www.sciencedirect.com/science/article/pii/B9780444527455000873.

[33] X. Chen, W. Shen, T. T. Vo, Z. Cao, and A. Kapoor, "An overview of lithium-ion batteries for electric vehicles," English, in *2012 10th International Power & Energy Conference (IPEC)*, ISSN: 1947-1270, Ho Chi Minh City, Vietnam: IEEE, Dec. 2012, pp. 230–235, ISBN: 978-1-4673-4584-2. DOI: 10.1109/ASSCC.2012.6523269. URL: https://ieeexplore.ieee.org/abstract/document/6523269?casa_token=XGgo-WGojEAAAAAA:x_50r6jvf83qPkI2pLfS0o4eMNpsj3zN4sxDusWVDzhioZQEvVIZqUeDa_5TDNaARKpoHCjtHRQ.

[34] J. Duan, X. Tang, H. Dai, Y. Yang, W. Wu, X. Wei, and Y. Huang, "Building Safe Lithium-Ion Batteries for Electric Vehicles: A Review," en, *Electrochemical Energy Reviews*, vol. 3, no. 1, pp. 1–42, Mar. 2020, ISSN: 2520-8136. DOI: 10.1007/s41918-019-00060-4. URL: https://doi.org/10.1007/s41918-019-00060-4.

[35] X. Han, M. Ouyang, L. Lu, and J. Li, "A comparative study of commercial lithium ion battery cycle life in electric vehicle: Capacity loss estimation," *Journal of Power Sources*, vol. 268, pp. 658–669, Dec. 2014, ISSN: 0378-7753. DOI: 10.1016/j.jpowsour.2014.06.111. URL: https://www.sciencedirect.com/science/article/pii/S0378775314009756.

[36] X. Zeng, M. Li, D. Abd El-Hady, W. Alshitari, A. S. Al-Bogami, J. Lu, and K. Amine, "Commercialization of Lithium Battery Technologies for Electric Vehicles," en, *Advanced Energy Materials*, vol. 9, no. 27, p. 1 900 161, 2019, _eprint: https://onlinelibrary.wiley.com/do ISSN: 1614-6840. DOI: 10.1002/aenm.201900161. URL: https://onlinelibrary.wiley.com/doi/abs/10.1002/aenm.201900161.

[37] D. Pavlov, *Lead-Acid Batteries: Science and Technology*, English. Elsevier, May 2011, ISBN: 978-0-08-093168-5.

[38] A. Einstein, *Relativity: The Special and the General Theory, a Popular Exposition*, English, trans. by R. W. Lawson. Methuen, 1931, Google-Books-ID: Dd8PAQAAMAAJ, ISBN: 978-0-416-37150-5.

[39] R. Ahuja, A. Blomqvist, P. Larsson, P. Pyykkö, and P. Zaleski-Ejgierd, "Relativity and the Lead-Acid Battery," *Physical Review Letters*, vol. 106, no. 1, p. 018 301, Jan. 2011, Publisher: American Physical Society. DOI: 10.1103/PhysRevLett.106.018301. URL: https://link.aps.org/doi/10.1103/PhysRevLett.106.018301.

[40] M. Yoshio, R. J. Brodd, and A. Kozawa, Eds., *Lithium-Ion Batteries: Science and Technologies*, en, 1st ed. New York, NY: Springer, 2009, ISBN: 978-0-387-34444-7 978-0-387-34445-4. DOI: 10.1007/978-0-387-34445-4. URL: https://link.springer.com/10.1007/978-0-387-34445-4.

[41] Battery University, *BU-205: Types of Lithium-ion*, en, Sep. 2010. URL: https://batteryuniversity.com/article/bu-205-types-of-lithium-ion.

[42] W. Vermeer, G. R. Chandra Mouli, and P. Bauer, "A Comprehensive Review on the Characteristics and Modeling of Lithium-Ion Battery Aging," *IEEE Transactions on Transportation Electrification*, vol. 8, no. 2, pp. 2205–2232, Jun. 2022, Conference Name: IEEE Transactions on Transportation Electrification, ISSN: 2332-7782. DOI: 10.1109/TTE.2021.3138357. URL: https://ieeexplore.ieee.org/abstract/document/9662298.

[43] T. Kim, W. Song, D.-Y. Son, L. K. Ono, and Y. Qi, "Lithium-ion batteries: Outlook on present, future, and hybridized technologies," en, *Journal of Materials Chemistry A*, vol. 7, no. 7, pp. 2942–2964, Feb. 2019, Publisher: The Royal Society of Chemistry, ISSN: 2050-7496. DOI: 10.1039/C8TA10513H. URL: https://pubs.rsc.org/en/content/articlelanding/2019/ta/c8ta10513h.

[44] M. Li, J. Lu, Z. Chen, and K. Amine, "30 Years of Lithium-Ion Batteries," en, *Advanced Materials*, vol. 30, no. 33, p. 1 800 561, 2018, _eprint: https://onlinelibrary.wiley.com/doi/pdf/10.1002 ISSN: 1521-4095. DOI: 10.1002/adma.201800561. URL: https://onlinelibrary.wiley.com/doi/abs/10.1002/adma.201800561.

[45] N. Nitta, F. Wu, J. T. Lee, and G. Yushin, "Li-ion battery materials: Present and future," *Materials Today*, vol. 18, no. 5, pp. 252–264, Jun. 2015, ISSN: 1369-7021. DOI: 10.1016/j.mattod.2014.10.040. URL: https://www.sciencedirect.com/science/article/pii/S1369702114004118.

[46] J. Jaguemont, L. Boulon, and Y. Dubé, "A comprehensive review of lithium-ion batteries used in hybrid and electric vehicles at cold temperatures," English, *Applied Energy*, vol. 164, pp. 99–114, Feb. 2016, ADS Bibcode: 2016ApEn..164...99J. DOI: 10.1016/j.apenergy.2015.11.034. URL: https://ui.adsabs.harvard.edu/abs/2016ApEn..164...99J.

[47] N. R. Chowdhury, A. J. Smith, K. Frenander, A. Mikheenkova, R. W. Lindström, and T. Thiringer, "Influence of state of charge window on the degradation of Tesla lithium-ion battery cells," *Journal of Energy Storage*, vol. 76, Jan. 2024, ISSN: 2352-152X. DOI: 10.1016/j.est.2023.110001. URL: https://www.sciencedirect.com/science/article/pii/S2352152X2303400X.

[48] EMRAX, *EMRAX 208 (86kW | 150Nm)*, 2024. URL: https://emrax.com/e-motors/emrax-208/.

[49] EMRAX, *EMRAX 188 (60kW | 100Nm)*, 2024. URL: https://emrax.com/e-motors/emrax-188/.

[50] Plettenberg, *NOVA 50 – Plettenberg*, 2024. URL: https://plettenbergmotors.com/product/nova-50-en/.

[51] EBMX, *EBMX XUB-80 Ultra Bee Motor and V2 Controller Bundle - EBMX Pty Ltd*, English. URL: https://ebmx.com.au/product/ebmx-ultra-bee-motor-and-controller-bundle/.

[52] Mot Energy, *ME1616 PMSM Water Cooled Motor*, 2011. URL: http://www.motenergy.com/mepmwaco.html.